

การวัดลักษณะลำอิเล็กทรอนิกส์ของเครื่องกำเนิดแสงสยาม

นายนพดล ดีแท้

วิทยานิพนธ์นี้เป็นส่วนหนึ่งของการศึกษาตามหลักสูตรปริญญาวิทยาศาสตรมหาบัณฑิต
สาขาวิชาฟิสิกส์
มหาวิทยาลัยเทคโนโลยีสุรนารี
ปีการศึกษา 2550

**ELECTRON BEAM PROFILE MEASUREMENT OF
THE SIAM PHOTON SOURCE**

Noppadon Deethae

**A Thesis Submitted in Partial Fulfillment of the Requirements for the
Degree of Master of Science in Physics
Suranaree University of Technology
Academic Year 2007**

ELECTRON BEAM PROFILE MEASUREMENT OF THE SIAM PHOTON SOURCE

Suranaree University of Technology has approved this thesis submitted in partial fulfillment of the requirements for a Master's Degree.

Thesis Examining Committee

(Asst. Prof. Dr. Chinorat Kobdaj)

Chairperson

(Dr. Saroj Rujirawat)

Member (Thesis Advisor)

(Asst. Prof. Dr. Prayoon Songsiriritthigul)

Member

(Asst. Prof. Dr. Supagorn Rugmai)

Member

(Dr. Prapong Klysuban)

Member

(Prof. Dr. Pairote Sattayatham)

Vice Rector for Academic Affairs

(Assoc. Prof. Dr. Prapan Manyum)

Dean of Institute of Science

นพดล ดีแท้ : การวัดลักษณะลำอิเล็กตรอนของเครื่องกำเนิดแสงสยาม (ELECTRON BEAM PROFILE MEASUREMENT OF THE SIAM PHOTON SOURCE) อาจารย์ที่ปรึกษา : ดร.สาโรช รุจิรวรรณ, 76 หน้า

ขนาดของลำอิเล็กตรอน ฟังก์ชันบีตาตรอน และค่าความเปล่งรังสี เป็นพารามิเตอร์ที่สำคัญสำหรับแหล่งกำเนิดแสงซินโครตรอน แหล่งกำเนิดแสงที่ดีจำเป็นต้องปรับการทำงานให้ค่าความเปล่งรังสีของลำอนุภาคน้อยที่สุดเท่าที่จะเป็นไปได้โดยค่าดังกล่าวจะสามารถคำนวณได้จากความสัมพันธ์ระหว่างฟังก์ชันบีตาตรอน และขนาดของลำอิเล็กตรอน ในงานศึกษาวิจัยนี้ได้ทำการพัฒนาระบบวัดขนาดของลำอิเล็กตรอน ที่เรียกว่า ระบบสร้างภาพรังสีเอกซ์ด้วยรูเข็ม(XPI) เพื่อใช้งานกับเครื่องกำเนิดแสงสยาม (SPS) ในการออกแบบได้ใช้หลักการทำงานของอุปกรณ์แบบเดียวกันกับหลักการทำงานของกล้องถ่ายภาพแบบรูเข็มเพียงแต่ใช้รังสีเอกซ์แทนที่แสงปกติเพื่อหลีกเลี่ยงขีดจำกัดการเลี้ยวเบนของแสง ซึ่งส่วนประกอบหลักของระบบโดยส่วนมากได้ถูกสร้างขึ้นเองภายในศูนย์ปฏิบัติการวิจัยเครื่องกำเนิดแสงซินโครตรอนแห่งชาติ ภายหลังจากการติดตั้งระบบ XPI ได้ถูกทดสอบการทำงานได้อย่างประสบความสำเร็จ สามารถสร้างภาพลำอิเล็กตรอนของ SPS ได้บนฉากเรืองแสงฟลูออเรสเซนต์ ซึ่งขนาดของลำอิเล็กตรอนสามารถหาได้จากการวิเคราะห์ภาพโดยลำอิเล็กตรอนของ SPS ที่พลังงาน 1.2 GeV ซึ่งมีขนาดในแนวนอนวัดได้ 403 μm และขนาดในแนวตั้งวัดได้ 128 μm ณ แม่เหล็กเลี้ยวเบนตัวที่ 2 และได้ทำการประมาณค่าความเปล่งรังสีของลำอิเล็กตรอนจากข้อมูลการวัดได้มีค่าเท่ากับ 83 nm rad ซึ่งเป็นค่าที่มากกว่าค่าที่ได้จากแบบจำลองเชิงทฤษฎีคือ 63 nm rad

สาขาวิชาฟิสิกส์
ปีการศึกษา 2550

ลายมือชื่อนักศึกษา _____
ลายมือชื่ออาจารย์ที่ปรึกษา _____

NOPPADON DEETHAE : ELECTRON BEAM PROFILE

MEASUREMENT OF THE SIAM PHOTON SOURCE. THESIS ADVISOR

: SAROJ RUJIRAWAT, Ph.D. 76 PP.

(BEAM DIAGNOSTICS/SYNCHROTRON RADIATION/X-RAY IMAGING)

Beam sizes, betatron functions and beam emittance are important parameters for synchrotron light sources. For a good light source, the beam emittance must be kept as low as possible. To obtain the beam emittance, the beam sizes and betatron functions must be known. In this thesis, an electron beam size measurement system called x-ray pinhole imaging (XPI) has been developed for the Siam Photon Source (SPS). The design was based on the working principle of a pinhole camera. The x-ray was used instead of visible light to avoid the diffraction limit. Most of the beamline main components were built in-house at the National Synchrotron Research Center. The XPI system was commissioned successfully. The synchrotron radiation x-ray image of electron beam was created on the fluorescence screen. From image analysis, the electron beam size was obtained. The measured horizontal natural beam size at the second bending magnet was $403\ \mu\text{m}$, and the measured vertical beam size was $128\ \mu\text{m}$ for the 1.2 GeV SPS storage ring. The horizontal beam emittance was determined to be $83\ \text{nm rad}$ which was higher than the theoretical value of $63\ \text{nm rad}$.

School of Physics

Student's Signature _____

Academic Year 2007

Advisor's Signature _____

ACKNOWLEDGEMENTS

I would like to express my gratitude to those who have contributed to the successful accomplishment of my thesis. First of all, the deeply thank Dr. Saroj Rujirawat, my thesis advisor who gives me opportunity to study in the graduate course in School of Physics of the Suranaree University of Technology and his great attention for me. Special thank to the head of the accelerator division of NSRC, Dr. Prapong Klysuban for supported of the Beryllium window and thanks Mr. Supan Boonsuya, Miss.Pikul Prawatsri and Mr. Pattanapong Junphuang, staff members of vacuum group of the NSRC for helpful to the XPI system design and installation.

I also would like to thank my thesis committee: Asst. Prof. Dr. Prayoon Songsiriritthigul, Asst. Prof. Dr. Supagorn Rugmai, Dr. Prapong Klysuban, Dr. Saroj Rujirawat, my thesis advisor and Asst. Prof. Dr. Chinorat kobdaj, the head of the school of physics. Last but not least, my parents for their sincerity encouragement.

I would also like to thank NSRC for the scholarship and the facilities for me to carry out this thesis.

Noppadon Deethae

CONTENTS

	Page
ABSTRACT IN THAI.....	I
ABSTRACT IN ENGLISH.....	II
ACKNOWLEDGEMENTS.....	III
CONTENTS.....	IV
LIST OF TABLES.....	VI
LIST OF FIGURES.....	VII
 CHAPTER	
I BACKGROUND.....	1
1.1 Properties of Synchrotron radiation.....	1
1.2 Siam Photon Source.....	3
1.3 SR production procedure.....	4
1.4 Motion of electron in storage ring.....	6
1.5 Siam Photon Source Parameters.....	13
1.5.1 SPS Beam parameters from Beam Optics.....	15
1.5.2 SPS Photon Spectrum.....	16
1.6 SR Beam diagnostic systems.....	17
1.6.1 Optical imaging of SR beam	17
1.6.2 X-ray pinhole imaging monitor.....	20
1.6.3 Synchrotron Radiation Interferometer.....	22

CONTENTS (Continued)

	Page
1.6.4 Streak camera.....	22
1.7 SR Beam diagnostic systems.....	23
II DESIGN AND CONTRUCTION OF THE XPI SYSTEM.....	25
2.1 General design of XPI.....	25
2.2 Ultra High Vacuum system.....	28
2.3 Beryllium window.....	33
2.4 X-ray pinhole.....	34
2.5 Fluorescent screen.....	35
2.6 Control system.....	36
2.7 X-ray image analysis system.....	38
III XPI COMMISSIONING AND EXPERIMENTS.....	41
3.1 Generation of x-ray beam image.....	41
3.2 Finding the real image size.....	43
3.3 Effect of pinhole aperture size.....	45
3.4 Beam images of different electron energy.....	46
3.5 Comparison of XPI and VLI.....	47
3.6 Finding of the natural beam size.....	48
3.7 Determination of beam emittance.....	49
3.8 XPI as the beam position monitor.....	50
IV CONCLUSION.....	52

CONTENTS (Continued)

	Page
REFERENCES.....	54
APPENDICES.....	56
APPENDIX A RESULTS FROM BEAM OPTICS CALCULATION.....	56
APPENDIX B DRAWING.....	63
APPENDIX C THE MATLAB BEAM ANALYSIS PROGRAM.....	70
CURRICULUM VITAE.....	76

LIST OF TABLES

Table	Page
1.1 SPS Basic parameters.....	12
1.2 STR Magnet parameters.....	13
2.1 Parameter for the pressure calculation.....	30
2.2 General properties of the beryllium window of the XPI system.....	33
2.3 General properties of the YAG:Ce screen.....	35
3.1 The SPS 1.2 GeV electron beam size at various beam currents.....	48
3.2 Machine parameters used in the determination of beam emittance.....	50
A1 Initial beam parameters.....	56
A2 Beam parameters list.....	56

LIST OF FIGURES

Figure	Page
1.1	Range of synchrotron radiation compared with the other light sources.....2
1.2	SR beam generated from bending magnet, wiggler and undulator.....2
1.3	The Siam Photon Source accelerator complex.....4
1.4	Production of synchrotron radiation from bending magnet.....5
1.5	Electrons make betatron oscillations along the central orbit.....8
1.6	Phase space ellipse and some beam parameters.....11
1.7	Result from Beam Optics calculation for the whole SPS 1.2 GeV ring.....14
1.8	Result from Beam Optics calculation for one super period.....15
1.9	SR spectrum produced from the bending magnet of SPS.....16
1.10	Schematics diagram of a SR optical beam imaging system.....18
1.11	Beam profile and the determination of beam FWHM.....18
1.12	Working principle of a pinhole camera.....20
1.13	The SRI system at SPring 8.....21
1.14	SR interference fringe from quad-slit of SPring 8 SRI.....22
1.15	Schematic diagram of a Hamamatsu streak camera.....23
2.1	Drawing of the vacuum chamber at BM2 of SPS storage ring.....26
2.2	General design layout for the XPI system.....26
2.3	The pressure distribution along vacuum tube between two vacuum pumps....29
2.4	Demonstration of UHV level in the first vacuum chamber.....30
2.5	Layout of the XPI vacuum component.....32

LIST OF FIGURES (Continued)

Figure	Page
2.6	Back side of the x-ray pinhole before mounting to the XPI system.....34
2.7	YAG:Ce fluorescent screen mounted on the copper holder.....36
2.8	The pinhole position driving stage mounted on the XPI beam line.....37
2.9	A touch screen display of XPI vacuum control system.....37
2.10	A raw x-ray beam image.....39
2.11	The output of XPI beam profile analysis program.....40
3.1	SR x-ray fan radiating on the pinhole.....42
3.2	Direct x-ray fan falling on the YAG:Ce screen.....42
3.3	The x-ray SR beam image formed on the YAG:Ce screen.....43
3.4	X-ray image on the YAG:Ce screen viewed from back side.....44
3.5	X-ray beam images taken with different pinhole aperture sizes.....45
3.6	X-ray beam images for different electron beam energies.....46
3.7	Comparison of x-ray and visible light beam images at a same condition.....47
3.8	The natural beam sizes can be obtained from linear relation of beam sizes and beam current. For SPS at 1.2 GeV, $\sigma_{0x} = 403 \mu\text{m}$ and $\sigma_{0y} = 128 \mu\text{m}$49
3.9	Electron beam position shifted cause by changing the RF frequency.....51
4.1	The new x-ray beam line at BL2 built by sharing the vacuum system with the XPI project.....53
B1	The vacuum chamber 1.....63
B2	The vacuum chamber 2.....64
B3	X-ray pinhole.....65

LIST OF FIGURES (Continued)

Figure		Page
B4	YAG screen support 1.....	66
B5	YAG screen support 2.....	67
B6	YAG screen support 3.....	68
B7	Long vacuum chamber tube.....	69

CHAPTER I

BACKGROUND

In this chapter, some background about synchrotron radiation, the Siam Photon Source, storage ring machine parameters and some beam diagnostic methods will be introduced.

1.1 Properties of Synchrotron radiation

Synchrotron radiation (SR) is a form of the electromagnetic wave emitted by relativistic electrons moving along a curving path under the influence of a magnetic field. SR was discovered in 1946 at the General Electric synchrotron in Schenectady (USA). At first, SR was named as “magnetic bremsstrahlung”. Shortly after the discovery of SR, J. Schwinger gave the SR production theory in 1946. (Kunz, 1979) However, it took some decades before researchers fully recognized that that SR has so many excellent properties suitable for experiments. At present, thousands of the researchers around the world are actively using SR on their experiments.

The unique properties of SR are:

1. SR spectrum covers broad band of electromagnetic wave, from infrared (IR) to hard x-ray regions.
2. SR source can supply brightness and highly collimated beams.
3. Linear polarization of SR parallel to the beam orbit plane.

4. Short bunch length in the order of nanosecond of time scale.

As shown in figure 1.1, synchrotron radiation has covered a broad range of electromagnetic spectrum from IR to x-rays.

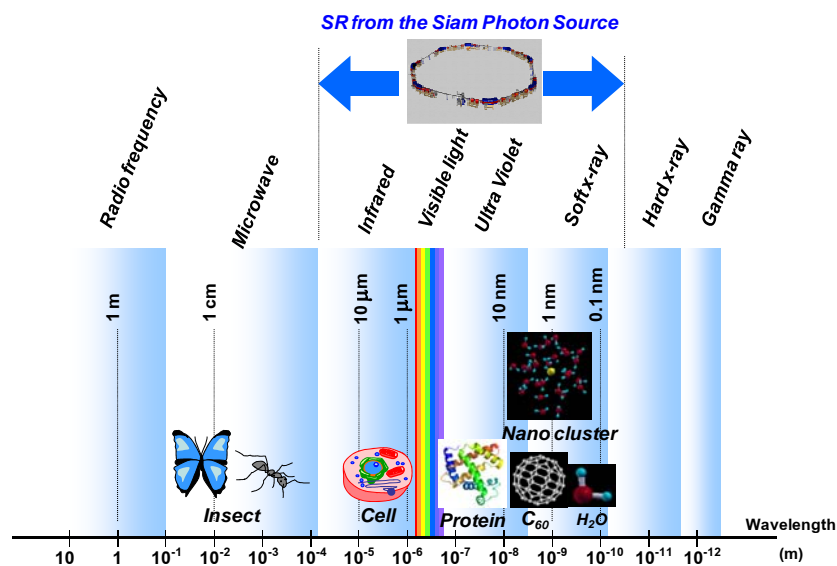


Figure 1.1 Range of synchrotron radiation compared with the other light sources.

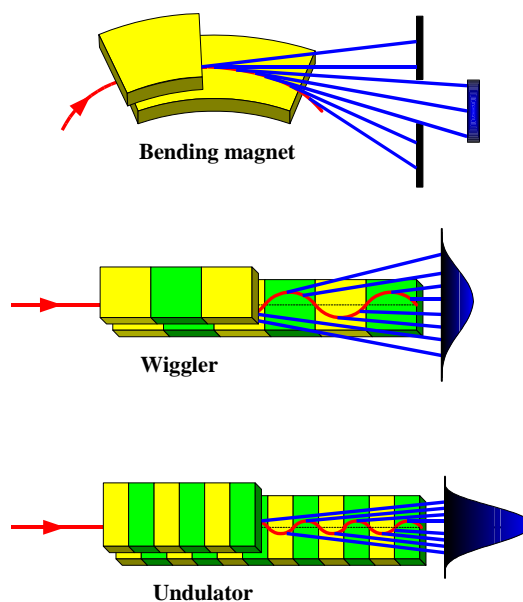


Figure 1.2 SR beam generated from bending magnet, wiggler and undulator

(Adapted from www.hasylab.desy.de)

Synchrotron radiation source or synchrotron light source is the heart of SR research facility. Normally, SR is produced by the *bending magnet* (BM) of the electron storage ring (STR). However, some special SR beams are produced by some addition devices called “insertion devices”, such as *undulator* and *wiggler*. The cartoon in figure 1.2 illustrates, SR beams generated from different devices. In this thesis, only the SR beam from bending magnet will be covered.

1.2 Siam Photon Source

The Siam Photon Source or SPS is the first and the only SR light source in Thailand. It is also the largest SR light source in south-east asia. After a long period of commissioning and hard working of people involved, this 1.2 GeV SR light source became operation-ready in 2004. Since then, SPS can supply SR beam to Thai researchers from several institutes with good reliability. The SPS has three main acceleration systems as illustrated in figure 1.3.

1. The linear accelerator or LINAC which can produce and accelerate the electrons up to the energy 40 MeV.
2. The booster synchrotron (SYN) which accelerates the electrons from LINAC up to the energy of 1 GeV.
3. The electron storage ring (STR) which is used to store the high energy electron from the Booster synchrotron and ramp the electron energy up to 1.2 GeV to produce the synchrotron radiation.

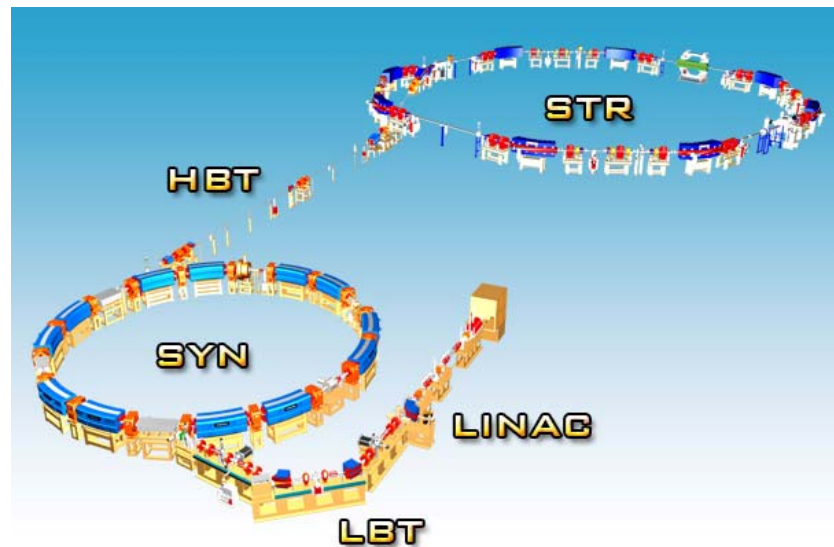


Figure 1.3 The Siam Photon Source accelerator complex (www.nsrc.or.th)

1.3 SR production procedure

The SR production procedure at SPS starts with electrons production by a conventional electron gun. Then electrons are accelerated by electric field in microwave through a 40 MeV LINAC. At this point, the relativistic electrons are transported through the low energy beam transport system (LBT) and fed to the Booster Synchrotron. The electron energy will be increased in SYN up to about 1 GeV. Then high energy electrons are extracted to the high energy beam transport system (HBT) and injected to the STR. The electron beam is maintained in STR in the form of electron bunches due to the nature of RF acceleration. The relativistic high energy electron production cycle is repeated every 2 seconds. Normally, it takes about 10 minutes to have STR filled with electron current of about 100 mA. Then the energy of STR is ramped from injection energy to 1.2 GeV. Finally after the electron orbit in STR has been corrected, the SR can be supplied to the users.

At present, the SR can be used continuously by users for more than 7 hours before the next STR refilling. Figure 1.4 depicts the SR production at a BM.

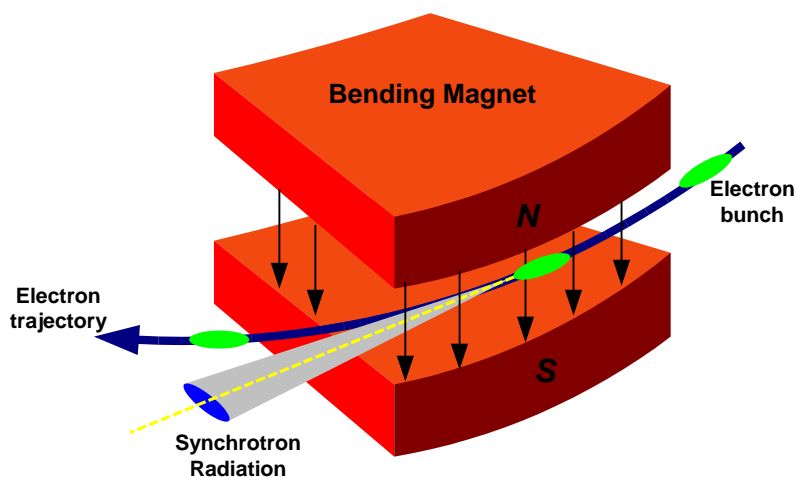


Figure 1.4 Production of synchrotron radiation from bending magnet

(Adapted from www.spring8.or.jp)

SR beam generated from STR is transported by beamline system to the experimental station which is installed at the front end of beamline. At present the SPS beam lines in operation are BL-4 for photo-emission, BL-6 for x-ray lithography and BL-8 for x-ray absorption applications. New beamlines under construction are PEEM-undulator and PX-wavelength shifter beamlines. Several more beamlines are planned for the near-future such as SAXS, IR and more XAS beamlines.

In order to fine-tune the performance of the SR light source or selection of the operation point, many importance machine parameters such as *beam emittance*, *betatron function* and *beam size* should be correctly determined. These parameters could be use to evaluate the performance of SR light source. One target of SR light source development is to get low *beam emittance* or small beam size which corresponding to high spectral brightness. During the user period, the stability and

intensity of light source are very important. Therefore, some beam monitoring and diagnostic systems are needed. Described in this thesis is the construction and testing of a STR diagnostic beam line at BL-2.

1.4 Motion of electron in storage ring

Along the electron orbit in STR, eight 45° BMs (BM1-BM8) are used for the deflection of electron beam to make full orbit. The bending magnet is a two poles magnet that generates uniform magnetic field. Obeying the Lorentz force law, relativistic electron motion path is bent by the bending magnet field and SR beam was emitted from the electron bunch under acceleration.

The SR beam fan is emitted from bending magnet along the tangential direction of electron motion path as shown in figure 1.3. In each BM, there is an almost uniform magnetic field B . The force \vec{F} acting on the moving electron is determined by the Lorentz's force. (Wiedemann, 1999)

$$\vec{F} = -e\vec{E} - e(\vec{v} \times \vec{B}) \quad (1.1)$$

where e is the electron charge, \vec{E} is the electric field and \vec{v} is the electron velocity.

The BM curvature radius (ρ) and the magnetic strength (B) of bending magnet are related to the electron energy (E) by

$$E[\text{GeV}] = 0.2998B[\text{T}]\rho[\text{m}] \quad (1.2)$$

The term $B\rho$ is called *beam rigidity*. For SPS, beam rigidity is 4.0 T m at the beam energy of 1.2 GeV.

According to the coulomb's law, the repulsive forces among electrons can cause the beam to spread out. There for some kind of magnets is needed for focusing the electron beam. One form of focusing magnet is *quadrupole magnet* (QM) which has four magnetic poles. In the center of QM, there is a magnetic field free region. This point defines the magnetic axis in the azimuthal direction along the orbit. Then the magnetic field changes linearly along the transverse direction in QM. The magnetic potential in QM is described by

$$V = -gxy \quad (1.3)$$

where g is the quadrupole gradient, x and y are horizontal and vertical positions transverse to the beam path.

The horizontal and vertical magnetic fields in QM are

$$B_x = -\frac{\partial V}{\partial x} = gy \quad \text{and} \quad B_y = -\frac{\partial V}{\partial y} = gx \quad (1.4)$$

The quadrupole gradient of field (g) is related to the electron energy by

$$g[\text{T/m}] = 3.3355 \frac{E[\text{GeV}]}{f L_{\text{eff}}} \quad (1.5)$$

where f is the focal length and L_{eff} is the magnetic field effective length of QM respectively. Normally two families of QM are used in STR, for focusing in both horizontal and vertical plans.

The quadrupole field strengths k is defined by

$$k = \frac{g}{B\rho} \quad (1.6)$$

And the focal length of quadrupole for thin-lens approximation is given by

$$f = \frac{1}{k \cdot L_{\text{eff}}} \quad (1.7)$$

If electrons in a bunch do not have the same energy then QM could not focus all of them into the focusing point. Similar to the correction of chromatic aberration in visible light optics, *sextupole magnet* (SM) is designed to correct the chromatic aberration of electron energy spread. This type of magnet is composed of six magnetic poles.

The focusing of electron beam and correction of chromatic aberration are causes of the electron oscillation around the reference or ideal orbit. This transverse oscillation is called *betatron oscillation* which occurs in the plane transverse to the trajectory of electron beam. The equation of betatron oscillation has the similar form to that of harmonic oscillation. The betatron oscillations in horizontal and vertical planes may be defined from the following equations of motion.

$$\frac{d^2}{ds^2}x(s) + K_x(s) \cdot x(s) = 0, \text{ and}$$

$$\frac{d^2}{ds^2}y(s) + K_y(s) \cdot y(s) = 0 \quad (1.8)$$

where s is the azimuthal coordinate, $x(s)$ and $y(s)$ are transverse coordinates as shown in figure 1.5.

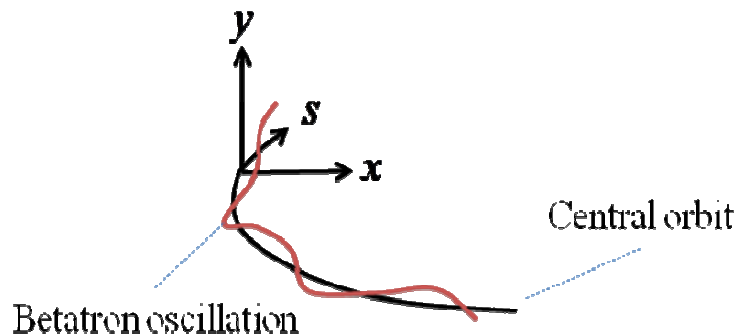


Figure 1.5 Electrons make betatron oscillations along the central orbit.

The focusing strengths $K_x(s)$ and $K_y(s)$ combine the quadrupole field strengths and weak focusing term $\frac{1}{\rho^2}$ and become zero in the magnetic field free region. In general

$$K_x(s) = k(s) + \frac{1}{\rho^2(s)}, \text{ and}$$

$$K_y(s) = k(s) \quad (1.9)$$

In 1958, Courants and Snyder showed that the solutions of equations (1.8) are:

$$x(s) = \sqrt{\varepsilon_x} \cdot \sqrt{\beta_x(s)} \cos(\psi_x(s) + \delta_{0x}), \text{ and}$$

$$y(s) = \sqrt{\varepsilon_y} \cdot \sqrt{\beta_y(s)} \cos(\psi_y(s) - \delta_{0y}) \quad (1.10)$$

where $\beta_x(s)$ and $\beta_y(s)$ are the *Betatron functions*, ε_x and ε_y are the *Emittances*.

$\psi_x(s)$ and $\psi_y(s)$ are the *Betatron phase angles*, δ_{0x} and δ_{0y} are initial phase angles.

The phase angles are defined by

$$\psi_x(s) = \int_{s_0}^s \frac{ds}{\beta_x(s)} \quad \text{and} \quad \psi_y(s) = \int_{s_0}^s \frac{ds}{\beta_y(s)} \quad (1.11)$$

From equations (1.10), it is quite obvious that the maximum amplitude of betatron oscillation of electrons at a given longitudinal position is proportional to the betatron function at that point.

$$x_{\max}(s) = \sqrt{\varepsilon_x} \cdot \sqrt{\beta_x(s)} \quad \text{and} \quad y_{\max}(s) = \sqrt{\varepsilon_y} \cdot \sqrt{\beta_y(s)} \quad (1.12)$$

Similarly, the maximum angles of the oscillation at a position are given by

$$x'_{\max}(s) = \sqrt{\varepsilon_x / \beta_x(s)} \quad \text{and} \quad y'_{\max}(s) = \sqrt{\varepsilon_y / \beta_y(s)} \quad (1.13)$$

Because betatron functions vary along the electron beam trajectory then the transverse electron beam envelope also depend on the azimuthal position. Due to the layout of magnets along the trajectory of electron beam, the betatron functions and the

beam envelop vary along the trajectory of electron beam. Accelerator scientists must keep the value of betatron functions within some limit otherwise the electron beam may scratch to the wall of STR vacuum chamber.

One of the important machine parameters which are used to indicate the operation point is the *Betatron tune*. The betatron tune is defined by the number of the betatron oscillation per one revolution. The betatron tunes in horizontal and vertical planes can be expressed as

$$\nu_x = \oint \frac{ds}{\beta_x(s)} \quad \text{and} \quad \nu_y = \oint \frac{ds}{\beta_y(s)} \quad (1.14)$$

Normally the betatron tunes and their combinations are chosen to be non-integer values to avoid beam lost in resonance when the trajectory repeat itself after some turns.

In figure 1.6, the locus of all possible positions and angle (x, x') of a particle that is going around the storage ring is plotted in phase space as an ellipse. It has been shown by Courants and Snyder (Wiedemann, 1999) that the area of the ellipse is

$$Area_{xy} = \varepsilon_{xy} \pi \quad (1.15)$$

where ε_{xy} denotes the emittance in horizontal or vertical plane. The shape and orientation of ellipse vary along the azimuthal position s but the area remains the same. When the ellipse represents the motion of electron in a bunch with the highest value of oscillation amplitude, ε_{xy} can be called *Beam emittance*.

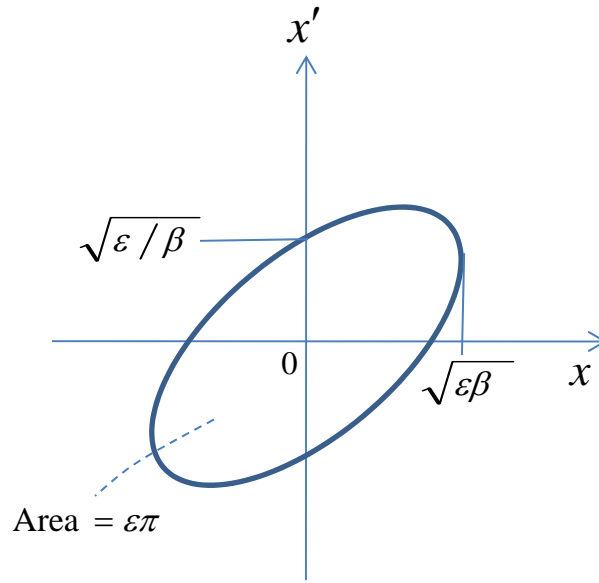


Figure 1.6 Phase space ellipse and some beam parameters (Duke, 2000)

In STR the distribution of betatron amplitude is Gaussian. The beam emittances are related to the standard deviation of amplitude distributions σ_x and σ_y by

$$\sigma_x = \sqrt{\epsilon_x \beta_x} \quad \text{and} \quad \sigma_y = \sqrt{\epsilon_y \beta_y} \quad (1.16)$$

The values σ_x and σ_y represent the Horizontal beam size and Vertical beam size respectively.

In the real situation, the electrons in beam do not have the same energy and their momentums are different. While the difference energy electrons passing through the bending magnet, electrons with higher energy will have smaller bending radius. This effect is called momentum dispersion. The dispersion amplitude of motion compared to the reference orbit is described by the *Dispersion function*(η). The magnetic field of BM is main effects of the Dispersion function in horizontal plane but it may be ignored in the vertical plane. The dispersion term to be added to the beam size is

$$x_\eta = \eta_x \frac{\Delta E}{E} \quad (1.17)$$

Then the beam sizes corrected by the dispersion function are

$$\sigma_x = \sqrt{\varepsilon_x \beta_x} + \eta_x \frac{\Delta E}{E} \quad \text{and} \quad \sigma_y = \sqrt{\varepsilon_y \beta_y} \quad (1.18)$$

If the beam sizes can be measured along with the betatron functions, then the beam emittance of SR source can be determined. (Wiedemann, 1999) In this work, the beam sizes of SPS are measured and analyzed by the instruments designed and built as parts of the thesis work.

1.5 Siam Photon Source Parameters

Some of the SPS parameters are showed in below. These parameters are used to model the SPS ring in the beam dynamic calculation program called *Beam Optics* developed by Prof. Helmut A. Wiedemann.




Table 1.1 SPS Basic parameters

Electron beam energy	1.2 GeV
Normal stored current	100 mA
Circumference of STR	81.3 m
Magnet lattice	Double Bend Achromat (DBA)
Super period	4
Length of a straight section	5.2 m
Betatron tune (ν_x / ν_y)	4.73/2.84

Beam emittance*	83 nm rad
RF frequency	118 MHz
Harmonic number	32
Energy lost per turn	65.94 keV
Critical energy of SR	1379 eV
Electron beam size (σ_x / σ_y)*	403 μ m/ 128 μ m

* Values from this work

Table 1.2 STR Magnet parameters

Bending magnet		
Bending field**	1.44 T	
Radius	2.78 m	
Bending angle	45°	
Quadrupole Magnet		
Quadrupole families	4 (8 QF1, 8 QD2, 8 QF3 and 8 QD4)	
Quadrupole gradients**	QF1 = 9.84 T/m, QF2 = -10.46 T/m QF3 = 9.25 T/m, QF4 = -7.00 T/m	
Effective length	0.323 m	
Sextupole Magnet		
Sextupole families	2 (8 SF and 4 SD)	
Sextupole fields**	SF = 74.2 T/m ² , SD = -79.8 T/m ²	

** The magnetic field at the position $x(s)$ along the beam orbit can be defined by the magnetic multipole expansion:

$$B(x(s)) = B_0(s) + gx(s) + \frac{1}{2}g'x^2 + \dots \quad (1.19)$$

where B_0 is the uniform bending field, g is the quadrupole field gradient, and g' is the sextupole gradient. (Wiedemann, 2002)

1.5.1 SPS Beam parameters from Beam Optics

Beam Optics code has been used for SPS beam dynamics modeling. The graphical output of main parameters shown in figure 1.7 and 1.8 are betatron functions (β_x, β_y) and the dispersion function (η_x). This model gives a value of horizontal beam emittance value of 63 nm rad. (Kawkasem, 2007) The beam parameter at the BM2 port are, $\beta_x = 1.958$ m, $\beta_y = 5.223$ m and $\eta = 0.132$ m

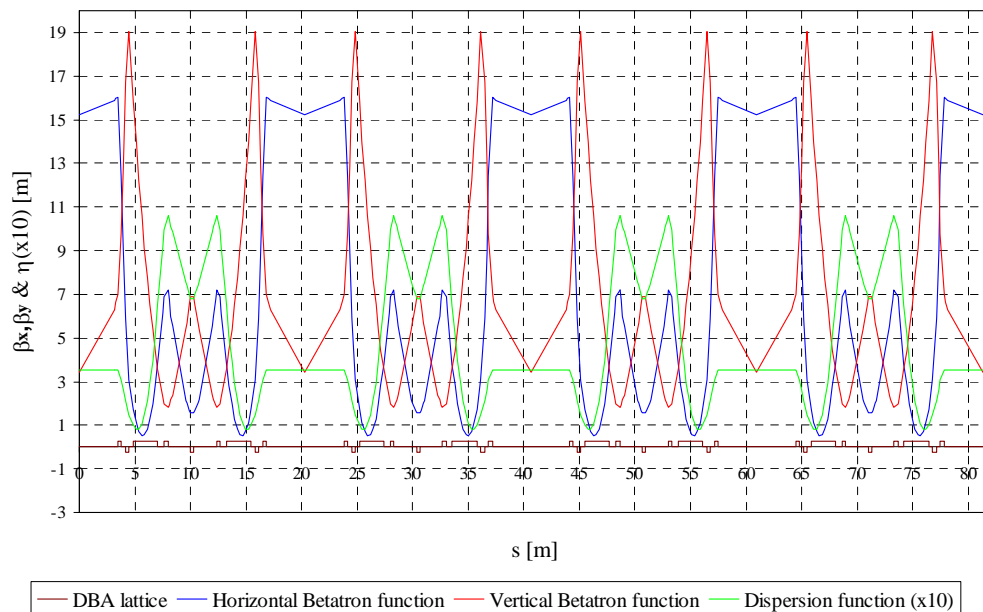


Figure 1.7 Result from Beam Optics calculation for the whole SPS 1.2 GeV ring

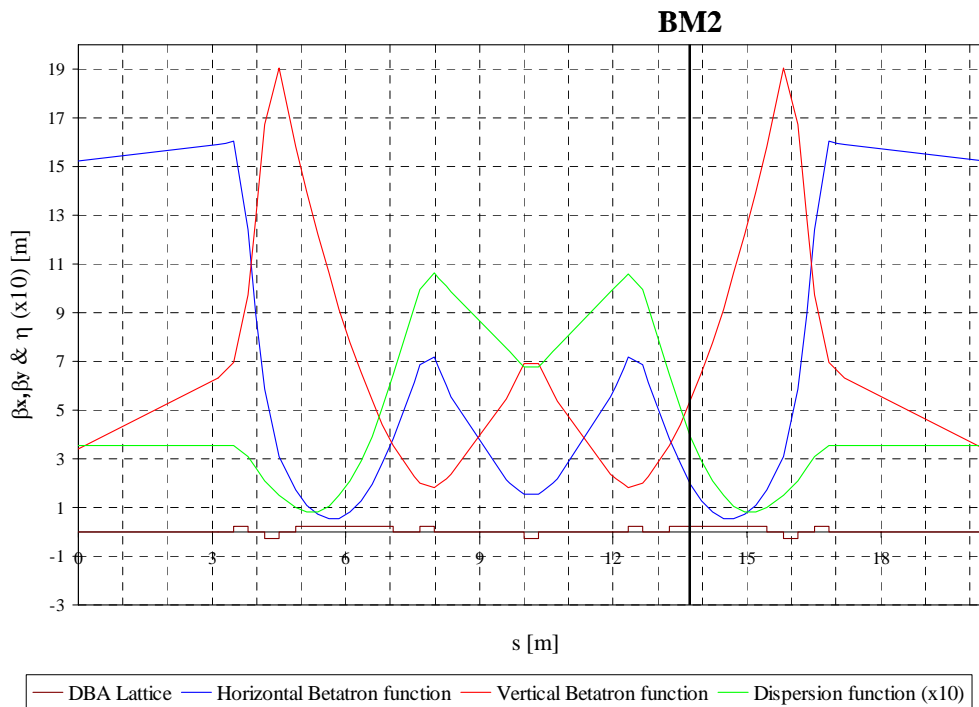


Figure 1.8 Result from Beam Optics calculation for one super period.

1.5.2 SPS Beam parameters from Beam Optics

The synchrotron radiation spectrum from the bending magnet of the Siam Photon Source is shown in figure 1.9 We used the SPECTRA 8.0 code developed at Spring 8 to calculate the flux density of the SPS synchrotron radiation from bending magnet. The machine parameters of the SPS described in the previous section are used for this calculation. In this work, the x-ray imaging system monitored the SR photon in the region above 1 keV (cut by beryllium window).

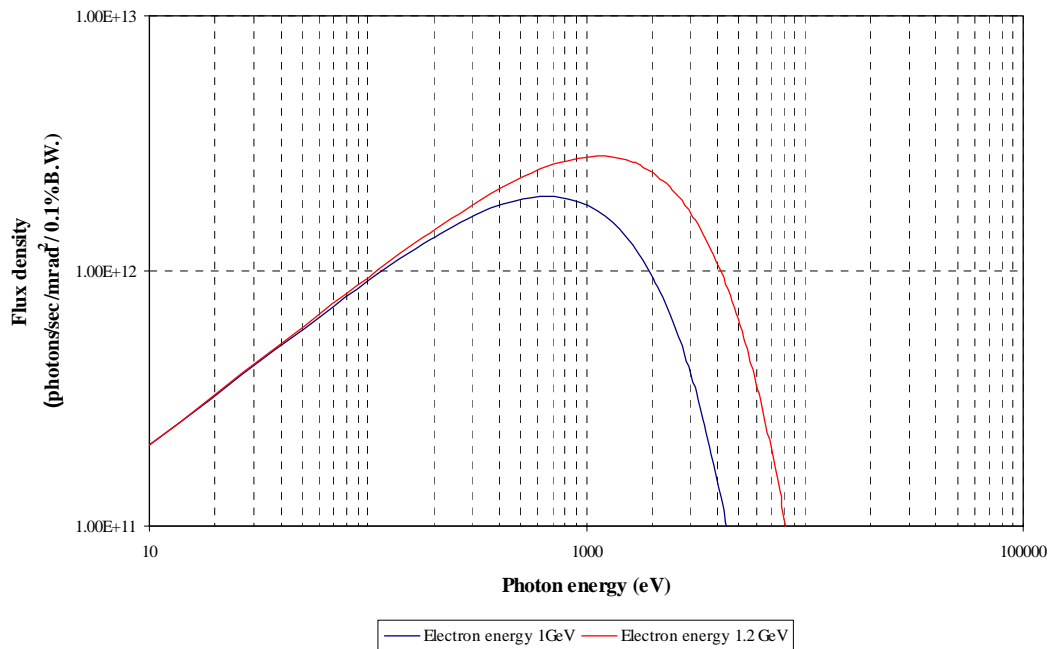


Figure 1.9 SR spectrum produced from the bending magnet of SPS

1.6 SR Beam diagnostic systems

The beam diagnostics system is a family of instruments used for *in situ* characterization of SR for the purposes of studying, control and improvement. In this section, some of the beam diagnostics systems used in synchrotron radiation facilities are described.

1.6.1 SPS Beam parameters from Beam Optics

The common SR beam diagnostic system used in SR light source is based on the optical imaging of SR beam. In general, SR is emitted from electron bunches tangentially to the trajectory in the bending magnet. If there is no focusing lens, SR image forms spread band on screen with a half-angle $\frac{1}{\gamma}$, where γ is the relativistic

factor. The focusing element is necessary to form electron beam image on screen. The transverse shape of electron bunches or *Beam profile* could be imaged by looking at the SR emission point. This is exactly the same way the astronomers used to study the shape of celestial bodies. This technique utilizes a telescope optical lens to direct the SR beam onto a screen or CCD camera forming the beam profile image. Some optical elements such as mirror, polarization plate, beam splitter, filters are also used to cut off x-ray, reduce the light intensity, remove the background and project light on the center of CCD. Normally, the optical elements are installed outside the vacuum chamber at the front end of beam line. The diagram of an SR optical beam imaging system is shown in figure 1.10. Magnification factor of this system can be calculated easily from single lens formula. By analysis of the beam image, the beam size could be directly calculated from the beam profile. Assuming that the SR radiation from electron bunch has Gaussian distribution, the full width at half maximum (FWHM) of the distribution could be determined from simple fitting. Since the beam size is the standard deviation of amplitude distributions, therefore it can be determined from FWHM of Gaussian distribution as (Kunz, 1979)

$$\sigma_{xy} \approx \frac{FWHM}{2.35} \quad (1.20)$$

Shown in figure 1.11 is an example of FWHM determination from SR beam profile image.

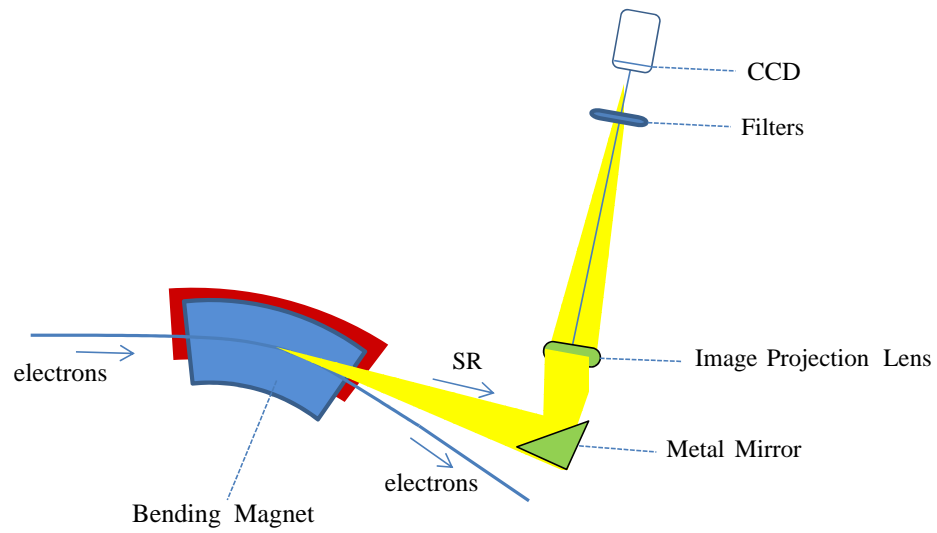


Figure 1.10 Schematics diagram of a SR optical beam imaging system.

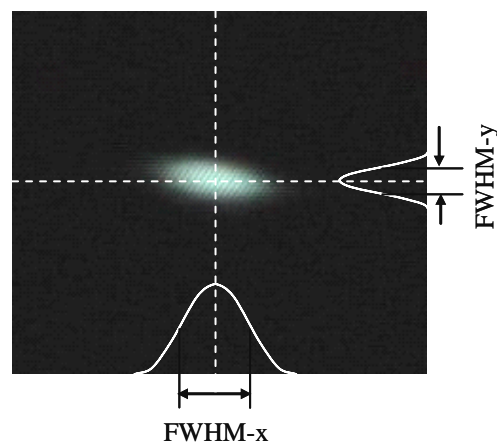


Figure 1.11 Beam profile and the determination of beam FWHM.

However, this technique is not suitable for very small electron beam measurement, due to diffraction nature of light. The resolution of an optical system which is located at a distance R from a point source may be determined by

$$d \approx \frac{\lambda R}{D} \quad (1.21)$$

where d is the distance between two point sources, D is the diameter of optical lens and λ is the wavelength of light used in the optical system. (Hecht, 2001) Suppose, a central wavelength of visible light of SR is 500 nm and the diameter of SR beam line aperture is 100 mm and optical lens is placed at a distance 1 m from the source, then minimum distance than this system can resolve is 5 μm . For SPS, the current beam size does not reach the resolution limit yet. However, for a new generation storage ring, the electron beam size may be much smaller and this method is not applicable. To avoid the diffraction limit the shorter wavelength must be used. In this thesis, we explore the beam imaging using SR in x-ray region and compare the result with the standard optical imaging.

1.6.2 X-ray pinhole imaging monitor

From the fact that the diffraction limit of x-ray is much smaller than the limits of UV or visible light, many SR facilities have utilized x-ray in their beam diagnostic system. The simplest system used is the x-ray pinhole camera. Figure 1.12 shows the general working principle of a pinhole camera. The pinhole is used to limit the field of view and direct light ray from object to the screen. The magnification factor of the system can be simply determined from the ratio between the distances between object to pinhole and the pinhole to screen. With this simplicity, optical ray tracing is not necessary in design and construction of such a system.

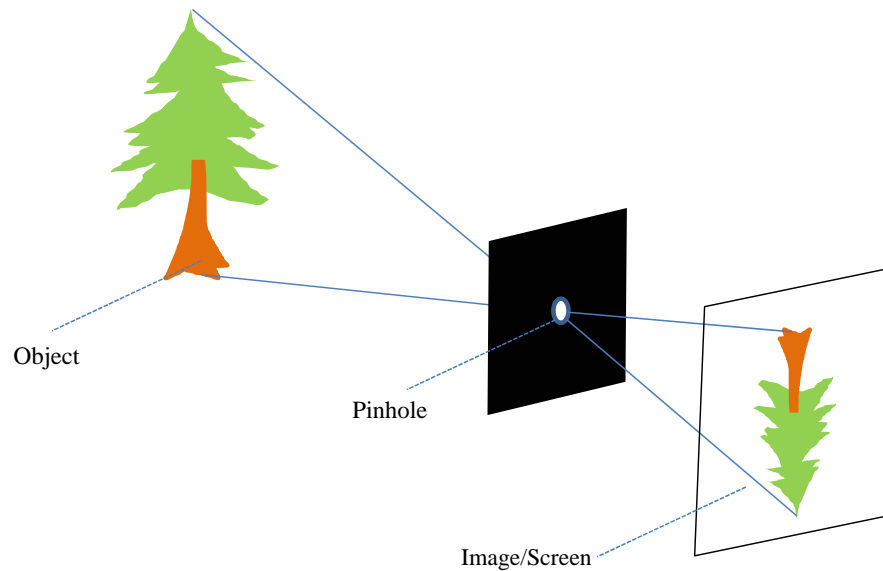


Figure 1.12 Working principle of a pinhole camera

An x-ray pinhole camera has been used at the SPEAR 2 storage ring in Stanford, USA. The tantalum x-ray pinhole has rectangular aperture size $30 \times 25 \mu\text{m}$. This system has been used successfully in the SPEAR 2 beam emittance reduction experiment. (Limborg, Safranek and Stefan, 2000) In this thesis, our x-ray pinhole imaging system uses a similar working principle. Many parts and materials are selected according to the information given in the work by Safranek et al. at SPEAR 2. The detail of design will be discussed in chapter II.

1.6.3 Synchrotron Radiation Interferometer

The use of direct beam imaging by visible light is hindered by the diffraction limit. However, there is a way to overcome this limit, by analyzing the diffraction pattern the information on the source size could be extracted. Synchrotron Radiation Interferometer (SRI) is one of the beam monitoring system for synchrotron radiation source. The working principle of SRI is similar to that of Michelson astronomical

interferometer which has been used in measurement of star diameter. One of the first of the SRI system was introduced by T. Mitsuhashi, et al. at a small SR light source in Ritsumeiken university, Japan. (Mitsuhashi, 1999) The diffraction limit and the aberration of lens which exist in visible light monitor are eliminated. The principal components of SRI system are double slit or quad slit and pattern projection lens.

Figure 1.13 shows the experiment setup of SRI system at SPring 8.

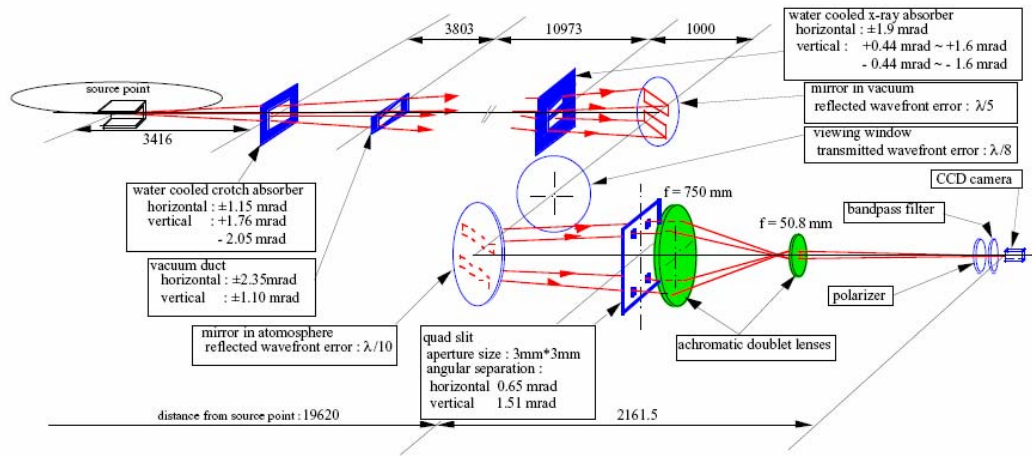


Figure 1.13 The SRI system at SPring 8 (Masaki and Takano, 2001)

In SRI, the visible monochromatic light from synchrotron radiation is diffracted by double slits or quad slit to create interference fringes on the screen. The relative intensity of the interference fringe on screen is transformed into a parameter named *Visibility*. For a quad slit, the interference fringe intensity such as shown in figure 1.14 is described by

$$I(x, y) = I_0 \left[\frac{\sin\left(\frac{\pi x a}{2\lambda L}\right)}{\frac{\pi x a}{2\lambda L}} \right]^2 \left[\frac{\sin\left(\frac{\pi y b}{2\lambda L}\right)}{\frac{\pi y b}{2\lambda L}} \right]^2 \left[1 + V_x \cos\left(\frac{4\pi x a}{\lambda L}\right) \right] \left[1 + V_y \cos\left(\frac{4\pi y b}{\lambda L}\right) \right] \quad (1.22)$$

Where a and b are the horizontal and vertical slit parameters, L is the distance from source to quad slit and λ is the wavelength of the monochromatic visible light. From the interference pattern, the values of visibility can be fitted using equation (1.22). Finally, the radiation source sizes can be obtained from Van Cittert Zernike theorem by the relations. (Masaki and Takano, 2001)

$$\sigma_x = \frac{\lambda}{2\pi\theta_x} \sqrt{-2\ln(V_x)}, \text{ and } \sigma_y = \frac{\lambda}{2\pi\theta_y} \sqrt{-2\ln(V_y)} \quad (1.23)$$

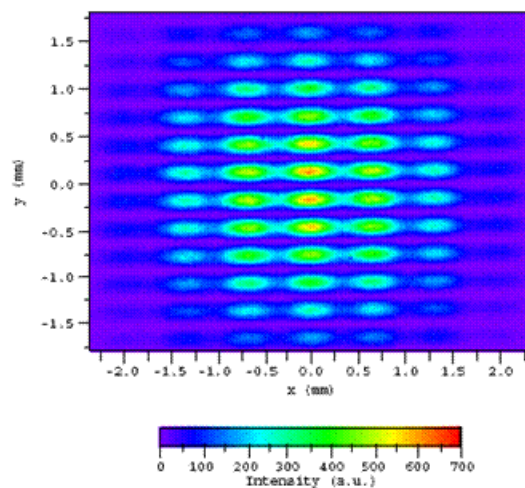


Figure 1.14 SR interference fringe from quad-slit of SPring 8 SRI

1.6.4 Streak camera

The streak camera is a high speed photo capturing instrument which is used widely in the laser and accelerator research such as laser pulse and longitudinal particle beam size measurements. A popular streak camera is produced by Hamamatsu. The schematic diagram of a Hamamatsu streak camera is shown in figure 1.15. The principle components in the streak tube are the photocathode (PC), sweep electrode pair, micro-channel plate (MCP) and phosphor screen.

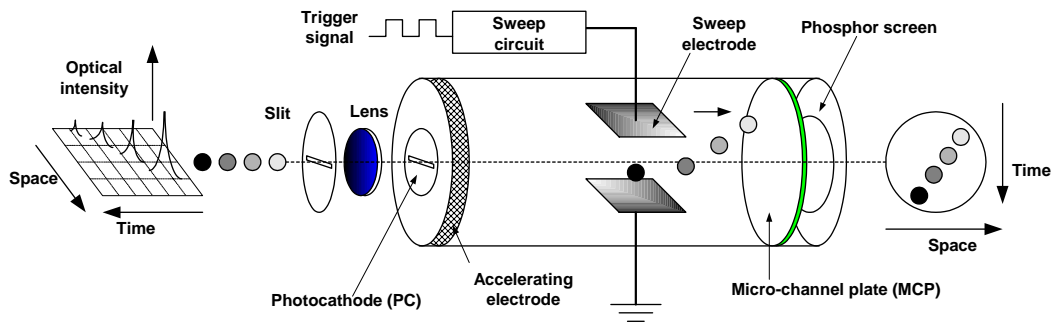


Figure 1.15 Schematic diagram of a Hamamatsu streak camera

(Adapted from www.hamamatsu.com)

The operating principle is fast pulse from the light source will be projected and focused by a slit and a lens to give an incident event on the PC of the streak tube. Photoelectrons which are released from the PC, come into sweep electrode pair operating in fast sweep rate. The number of photoelectron is proportional to the light's intensity thus the image on the fluorescent screen indicates the temporal beam profile. To get a better image intensity, the photoelectrons signal in the streak tube may be amplified by using the MCP before incident onto the fluorescence screen. For longitudinal SR beam size measurement, it may be necessary to use a streak camera, which is not in the scope of this work.

1.7 Purpose of work

In this thesis, the beam size instrumentation and measurement are limited to the case of the XPI system. The instrumentation includes design, components fabrication, installation, programming, and commissioning. In beam size measurement, the raw image data is used to extract the horizontal and vertical beam sizes. The STR parameter from a beam dynamics model that gives the horizontal

emittance of 63 nm rad is used as the reference. The other parameters necessary for the calculation are also supported by the members of NSRC accelerator division. The aims of the work described in this thesis are:

1. To study the principle of electron beam profile measurement in detail.
2. To compare the performance between different types of beam monitoring system (optical imaging versus x-ray imaging).
3. To participate in the design, fabricate, install and test of a new beam monitoring system of SPS.
4. To measure the electron beam size and estimate the electron beam emittance for the SPS storage ring.

In the next chapter, the design and component fabrication of the x-ray pinhole imaging system are described.

CHAPTER II

DESIGN AND CONSTRUCTION OF XPI SYSTEM

Presented in this chapter are the design and construction of XPI system to be used with SPS storage ring. The topics are general design, vacuum system, beryllium window, the x-ray pinhole with variable aperture size, fluorescent screen, control system and image analysis program.

2.1 General design of XPI

The synchrotron radiation (SR) from the bending magnet is emitted as radiation cone through the opening angle of vacuum chamber beam port. The opening angle of the radiation beam itself is provided by the relativistic factor. For SPS at 1.2 GeV the factor is $\gamma = 2348$. The beam opening angle is given by $\frac{1}{\gamma} \approx 0.4 \text{ mrad}$. All of the optical components of XPI system must be placed in a straight line within this small opening angle. The trade-off for the simple optical design for pinhole system is the difficulty in alignment of optical alignment, especially for the components placed in vacuum. The pinhole aperture and screen must be placed in the same straight line along the center of SR cone from the source point. Since the source point is not necessary at the ideal central orbit, the design must include the flexibility of in-vacuum position adjustment for those simple optical elements. In a normal SPS bending magnet BM2, the bending port of vacuum chamber is made for the source

point at 10° bending angle as shown in a drawing of vacuum bending chamber in figure 2.1.

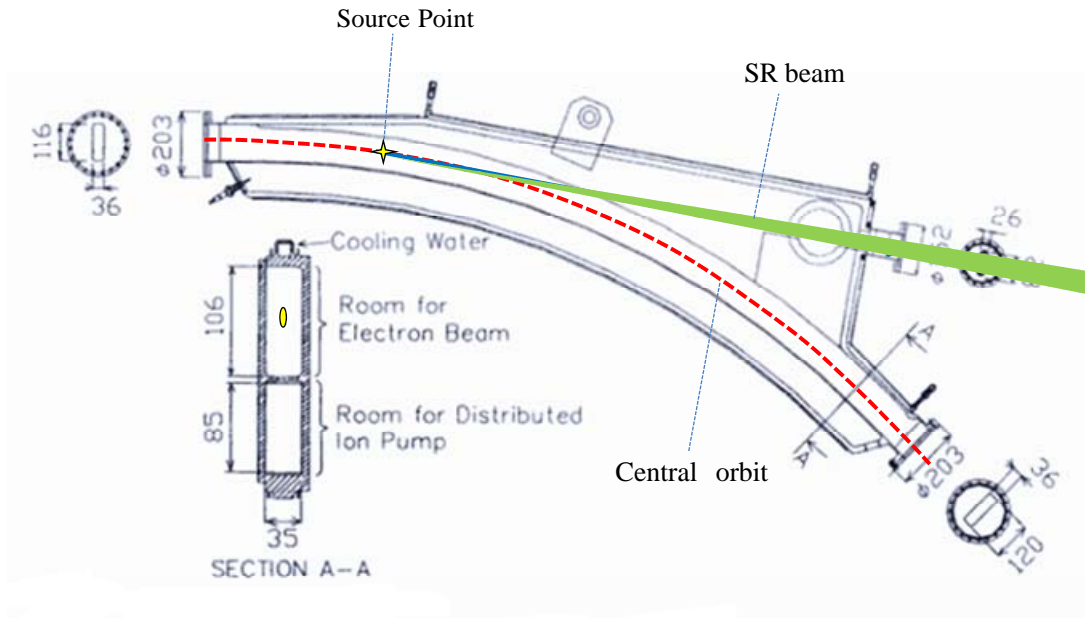


Figure 2.1 Drawing of the vacuum chamber at BM2 of SPS storage ring

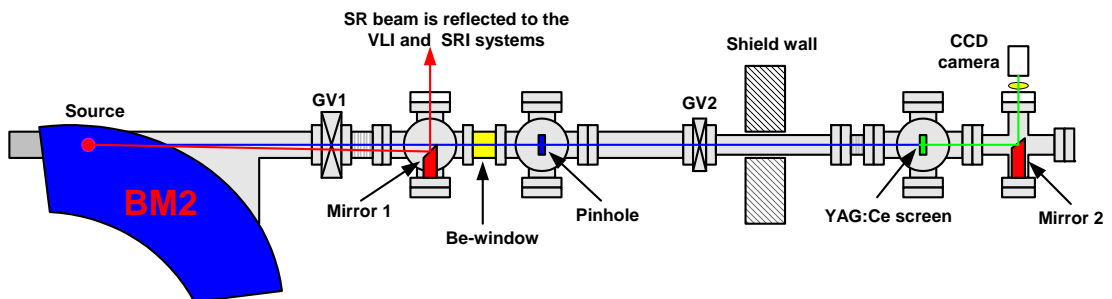


Figure 2.2 General design layout for the XPI system

In our general design criteria, we wish to compare the visible light imaging (VLI) and x-ray pinhole imaging (XPI), therefore the system must be capable to operate in both visible and x-ray region. Figure 2.2 shows a general design layout for SPS XPI system. The vacuum gate valve, GV1, is placed at the beam port of bending

chamber for vacuum isolation during installation. The first vacuum chamber is used to house a metal mirror (M1). This mirror is used for reflecting the visible region of SR from source point through to a view glass vacuum window for VLI system. The future SRI system could also use SR from this part. Next to the first chamber is a commercial beryllium (Be) window for filter-out the visible and UV from SR x-ray and for vacuum isolation. The x-ray pinhole is placed in the second vacuum chamber, right after the Be window. This pinhole is made from tantalum blades attached to copper base which has cooling water running through. The aperture of x-ray pinhole is adjustable (not in vacuum) to as low as $30\ \mu\text{m} \times 30\ \mu\text{m}$. The whole pinhole assembly can be moved in vertical direction by a vacuum feed-through motorized stage for alignment purpose. Next to the second chamber are the first vacuum tube, second gate valve GV2, and another vacuum tube for making x-ray optical path through the radiation shield wall. A vacuum bellow is placed after the last vacuum duct to enable position adjustment. The third vacuum chamber is placed after the bellow. A Ce-doped YAG fluorescent screen is placed inside the third chamber. The SR x-ray image will be formed on the Ce:YAG screen, converting x-ray into visible light using fluorescence process. The beam image is viewed by a CCD camera using reflection of light through an end mirror (M2) and a vacuum viewport. The image is analyzed by a simple algorithm based on MATLAB program. By this way, the electron beam sizes and beam position can be measured using the XPI system.

2.2 Ultra High Vacuum system

The good vacuum level of XPI system is essential because it is connected directly to the SPS storage ring. In STR the vacuum level is maintained in the ultra high vacuum (UHV) level or the average pressure is in the range of 10^{-10} Torr. We use three refurbished, 500 l/s sputtering ion pumps (SIPs) to maintain the vacuum level throughout the beamline. In our design, the first vacuum chamber is maintained by the first SIP in the same UHV level as the SPS STR (10^{-10} Torr). For the first chamber, the vacuum baking process is used to achieve the UHV level. The vacuum in the second chamber is separated from the first chamber by the Be window. We use the second SIP to maintain the vacuum level in the second chamber to be around 10^{-9} Torr. From the second chamber to the third chamber, there is a long SR beam path in vacuum. At this stage through the end of beamline, the vacuum level is maintained by the last SIP to be around 10^{-8} Torr. The SIPs and vacuum gauges are connected to a vacuum control system based on PLC technology developed by NSRC staffs.

All of the vacuum chambers are fabricated by the machine shop of NSRC. After the fabrication all of the vacuum components went through the chemical cleaning processes. Leak testing of vacuum components was done in the NSRC vacuum shop. Helium leak test of all vacuum components such as vacuum chambers, welding joints, bellows, gate valves, vacuum gauges, feed-through and adapters was performed to ensure the leak free condition. Drawings of components used in the constructed XPI system are compiled in the appendix.

To estimate the maximum pressure and average pressure of the XPI beamline between the second chamber and the third chamber we use the formula

$$P_{\max} = Aq\left(\frac{L^2}{4C} + \frac{L}{S}\right) \quad (2.1)$$

and

$$P_{av} = Aq\left(\frac{L^2}{6C} + \frac{L}{S}\right) \quad (2.2)$$

where A is the specific surface area (m^2), q is the specific outgassing rate (mbar l/s cm^2), L is the distance between pumps, S is the effective pumping speed (l/s) and C is the tube conductance (m^3/s). (Turner, 1999) Figure 2.3 shows a sketch of pressure distribution between two adjacent pumps.

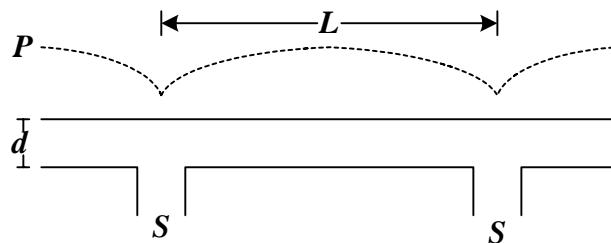


Figure 2.3 The pressure distribution along vacuum tube between two vacuum pumps

For the cylindrical tube, the conductance can be estimated by

$$C = 305 \frac{d^3}{L} \sqrt{\frac{T}{M}} \quad (2.3)$$

where d is the diameter (m), L is the length (m), T is the temperature (K) and M is the molecular weight of gas which means hydrogen ($M_{\text{H}_2}=2$). (Turner, 1999)

The effective pumping speed can be estimated from

$$\frac{1}{S} = \frac{1}{S_o} + \frac{1}{C} \quad (2.4)$$

where S_o is the nominal pumping speed (l/s), C is the conductance ($\text{mbar l}^2 \text{ s}^{-1} \text{ cm}^{-2}$)

The vacuum parameters used in XPI pressure estimation are shown in table 2.1. (Turner, 1999)

Table 2.1 Parameter for the pressure calculation

Parameters	
Molecule gas	H ₂
Nominal pumping speed of ion sputter pump (l/s)	500
Temperature (K)	300
Distance between pumps (m)	4.92
H ₂ outgassing rate for SUS304 (mbar l/ s cm ²)	10 ⁻¹¹
Average diameter (m)	0.097
Average area (m ²)	1.69

From the parameters and equation above we have estimated the maximum and average vacuum pressures in the XPI system to be 2.01×10^{-9} Torr and 1.64×10^{-9} Torr, which are good enough to serve our purpose. Shown in figure 2.4 is the demonstration of UHV level achievable in the NSRC-made first XPI vacuum chamber. The layout of the XPI vacuum component is shown in figure 2.5



Figure 2.4 Demonstration of UHV level in the first vacuum chamber

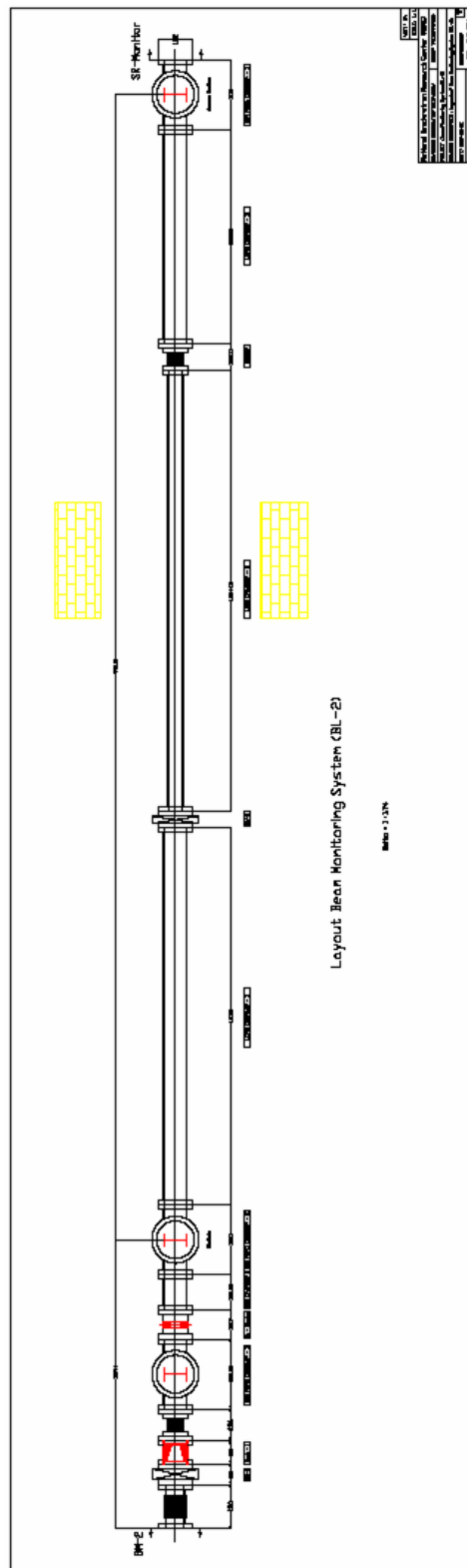


Figure 2.5 Layout of the XPI vacuum component

2.3 Beryllium window

The beryllium (Be) window is used to separate the vacuum of STR from the most of XPI vacuum for safety purpose. Since it is a light element, Be is quite transparent to x-ray. In this work we use a Be-window for cutting the UV and visible light from x-ray in XPI system. This window used to be the spare part of the LIGA beamline project. The general properties of the beryllium window are shown in table 2.2 (www.berylliumproducts.com)

Table 2.2 General properties of the beryllium window of the XPI system.

Properties	
Material	Beryllium 99%
Thickness (in)	0.004
Aperture dimension (mm ²)	800
Type	PF-60 Diffusion bonding
Window coating	Duracoat
Fractional transmittances	0.964
Density (lb/in ³)	0.066
Melting point (°F)	2350
Special heat (Btu/lb °F)	0.42
Thermal conductivity (Btu ft/ft ² hr-°F)	105
Electrical resistivity (μΩ/cm)	41
Operating time at vacuum environment	10 year

2.4 X-ray pinhole

The x-ray pinhole is the heart of XPI system. The pinhole aperture was design to have rectangular shape for the convenient of size adjustment. The aperture was made from two pairs of tantalum plates. Each pair of tantalum plate is mounted diagonally to the other on a copper base. The tantalum edge was sliced to make good well-defined square aperture. The copper base is connected to the water cooling tubes feeding through a motion feed-through attached on vacuum flange and bellow. The diameter of aperture was measured by simple diffraction technique using a He-Ne laser (wavelength 632.8 nm). For beam size measurements, the square apertures were adjusted to be 30 μm , 50 μm and 75 μm , respectively. The whole pinhole and motion feed through are made using the NSRC in-house technology. Figure 2.6 is a photo of x-ray pinhole used in this work.

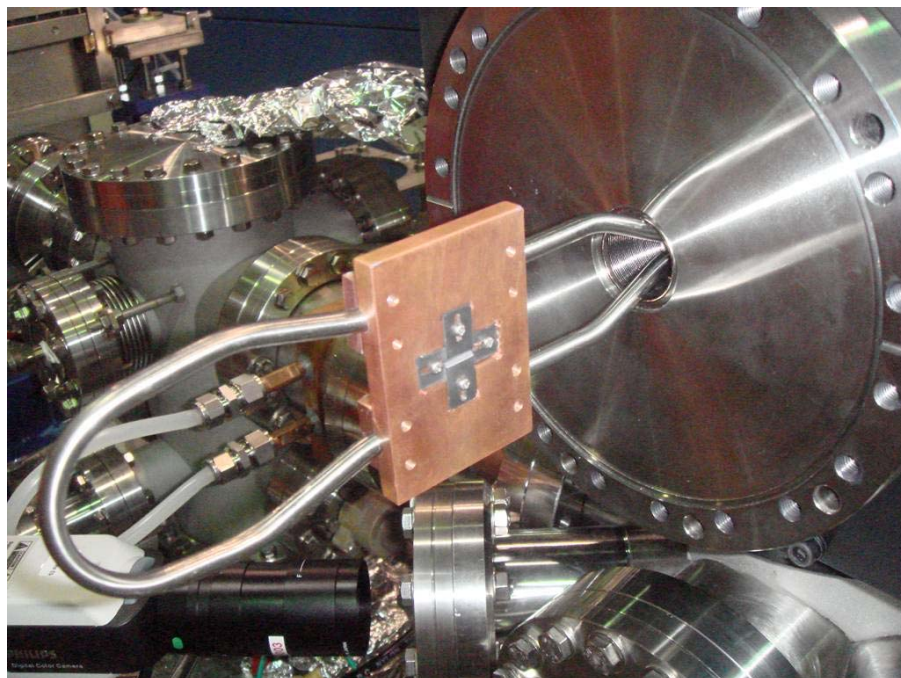


Figure 2.6 Back size of the x-ray pinhole before mounting to the XPI system

2.5 Fluorescent screen

SR x-ray is projected by the x-ray pinhole onto the fluorescent screen to make the x-ray beam image. At the screen, the x-ray image become visible due to the x-ray induced fluorescent process. The yttrium aluminum garnet crystal ($Y_3Al_5O_{12}$) doped with cerium (YAG:Ce) is a very sensitive fluorescence material. Moreover, this crystal is transparent to the visible light thus allowing observation from backside. This crystal was selected for the XPI system of SPEAR 2. (Limborg, Safranek and Stefan, 2000) The general properties of YAG:Ce screen used in this work are shown in table 2.3. (www.bnl.gov) Shown in figure 2.7 is the photo of the YAG:Ce screen mounted on the copper holder, to be placed in the third vacuum chamber.

Table 2.3 General properties of the YAG:Ce screen

Properties	
Crystal color	Yellow
Diameter (mm)	13
Thickness (mm)	0.5
Index of refraction	1.82
Wavelength of peak emission (nm)	550
Density (g/cm^3)	4.57
Photon yield (# photon/MeV)	8×10^3
Scintillation efficiency (%)	15
Cerium concentration (%)	0.18

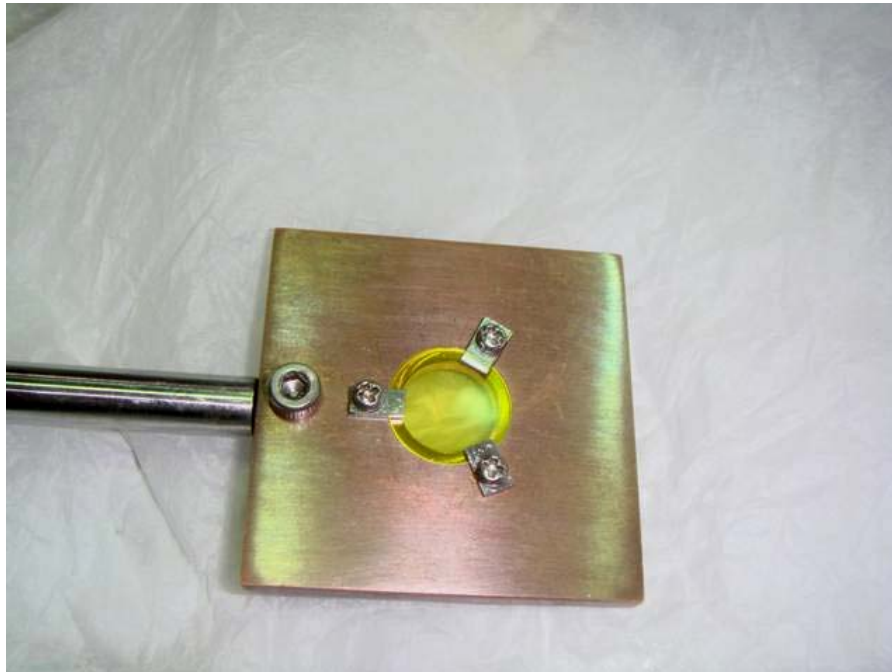


Figure 2.7 YAG:Ce fluorescence screen mounted on the copper holder

2.6 Control system

The control system of XPI is separated into two subsystems. The first one is for pinhole position movement and the second one is for vacuum and interlock control system. Both subsystems were designed to operate in the manual (remote) control mode or automatic control mode. The vertical position of pinhole can be controlled by using a step motor to drive the pinhole axis in the vertical direction. The step motor control system is developed by NSRC staffs. Figure 2.8 is a photo showing the pinhole axis positioning stage and some components mounted on the beam line. By this way, the vertical position of pinhole can be controlled with the accuracy as small as 10 μm .

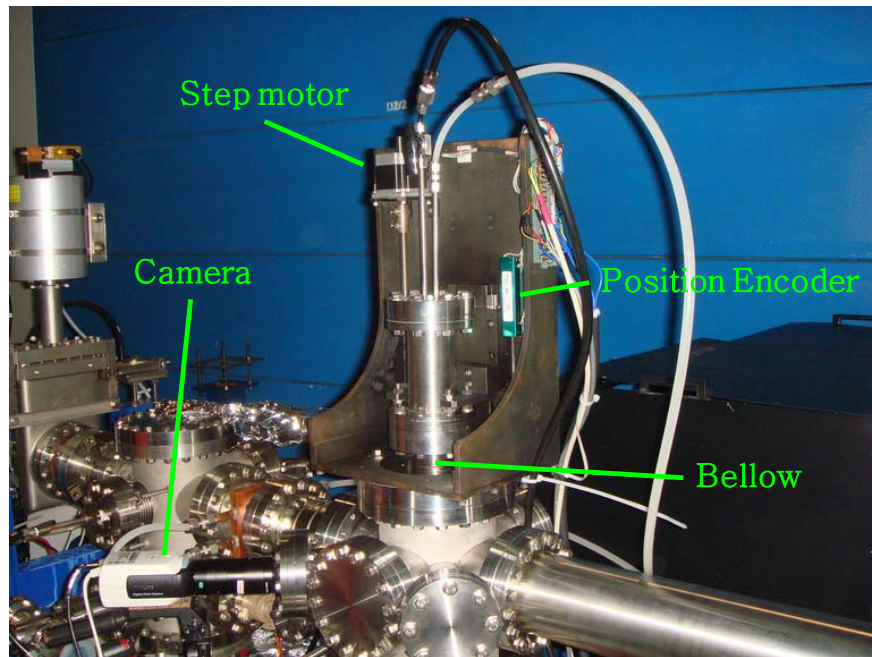


Figure 2.8 The pinhole position driving stage mounted on the XPI beam line

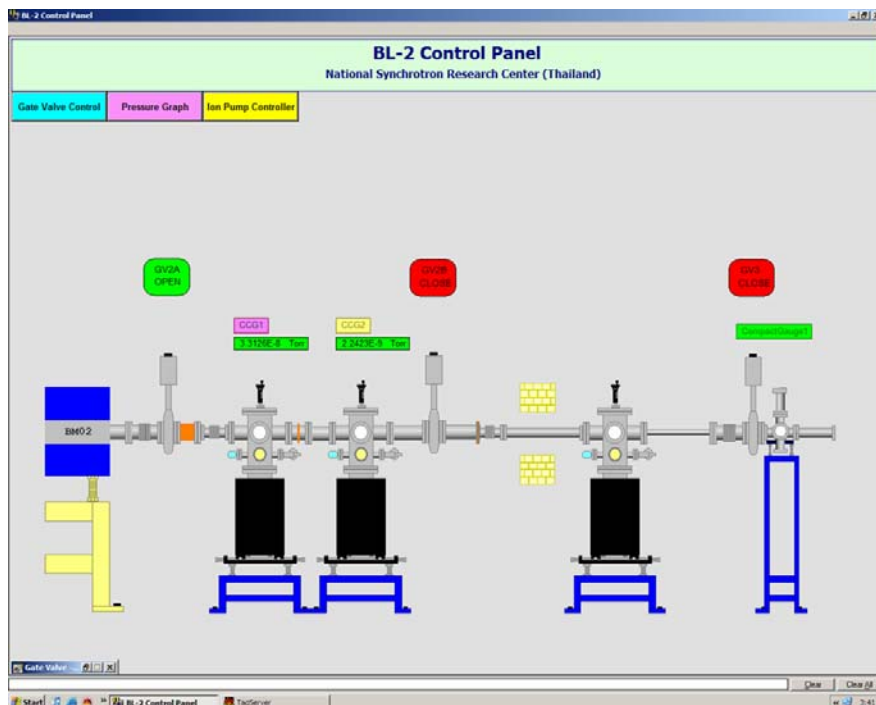


Figure 2.9 A touch screen display of XPI vacuum control system

For vacuum system controlling, a control system based on PLC technology has been developed by a NSRC staff. This system can monitor the vacuum level of the XPI vacuum chambers and control the motion of gate valve for vacuum interlock purpose. The first gate valve connected to the storage ring will not open if the pressure of first vacuum chamber is not in the UHV level. The other gate valve is programmed to protect the second SIPs in the case of fatal leak occur in the downstream end of beam line. For the convenient of beam line user, the control system is design to have a touch screen control and display. Figure 2.9 shows the display of the vacuum control of the XPI beam line.

2.7 X-ray image analysis system

The x-ray beam image appeared on the YAG:Ce screen is taken by the CCD camera in backside viewing. By using, a flat mirror (M2) the beam image can be reflected into the CCD camera mounted on a view port of the third vacuum chamber. The x-ray beam image is transferred to a personal computer via a coaxial cable. An IMAQ image processing card is used for image capturing. The format of the x-ray beam image is set to 768x576 pixels, 32 bits RGB image file. Shown in figure 2.10 is a raw x-ray beam image captured by the system.



Figure 2.10 A raw x-ray beam image

After capturing, the x-ray beam image must be analyzed to extract the beam size parameters. Since the size of fluorescent screen is known, then the beam sizes of x-ray image could be measured directly using a simple calibration factor. To get the real beam size, the magnification factor of XPI system is put in calculation. The real x-ray beam size can be calculated easily using the beam size of x-ray image divided by the magnification factor. A simple MATLAB code is written for this purpose. The Gaussian distribution is fitted to the beam horizontal and vertical profiles to give FWHMs. By using equation (1.20), the beam sizes are calculated directly from the FWHMs of the Gaussian fitting. The graphical output of beam size measurement program is shown in figure 2.11.

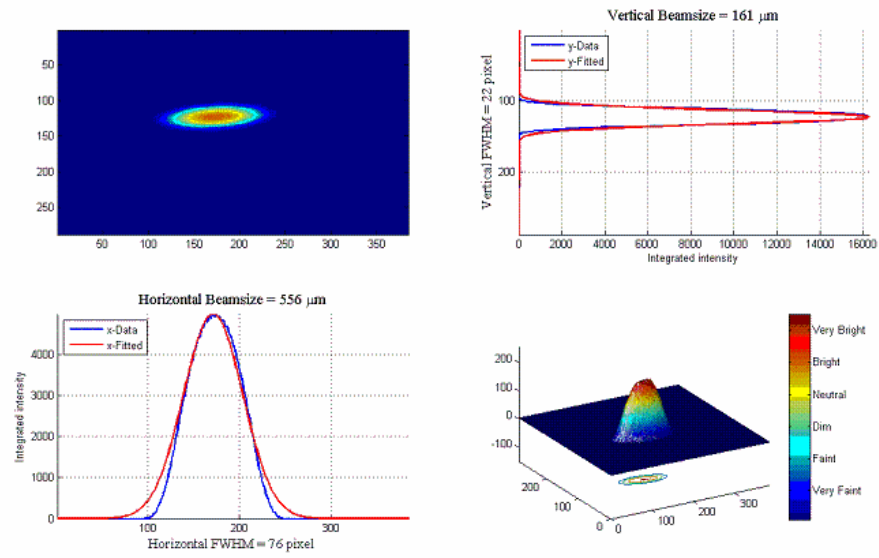


Figure 2.11 The output of XPI beam profile analysis program

In the next chapter, the result of XPI commissioning and some beam measurement results are presented.

CHAPTER III

XPI COMMISSIONING AND EXPERIMENTS

3.1 Generation of X-ray beam image

As discussed in the last chapter, the simple optical design of XPI led to difficulties in beam alignment. To generate the x-ray beam image on the fluorescent screen, the x-ray pinhole and the screen must be placed onto the optical axis. In this case, the optical axis is defined as a single straight line along the direction of central SR line originated from the source point. The most difficult part was to place the pinhole aperture on the optical axis. As shown in figure 3.1, the SR x-ray fan radiating on the pinhole. The x-ray trace is made visible by coating the front side of pinhole base with phosphor powder. The x-ray trace ensures that the pinhole vertical direction is in the radiation plan. The optical axis lies on this plan, however, to find the axis one has to align the source, the pinhole and the image. In reality, it is not easy to align three points on independent components to be right on one single straight line, especially when the three points are in vacuum. Since the pinhole is not designed to move in horizontal direction, the whole vacuum chamber has to be moved in order to align the pinhole on the optical axis. The beam alignment was performed when STR was running at low current (2-3 mA) for safety purpose, since it can be done only inside the radiation shield wall. With the help of CCD cameras and several NSRC staffs involved, the x-ray beam alignment could be done.

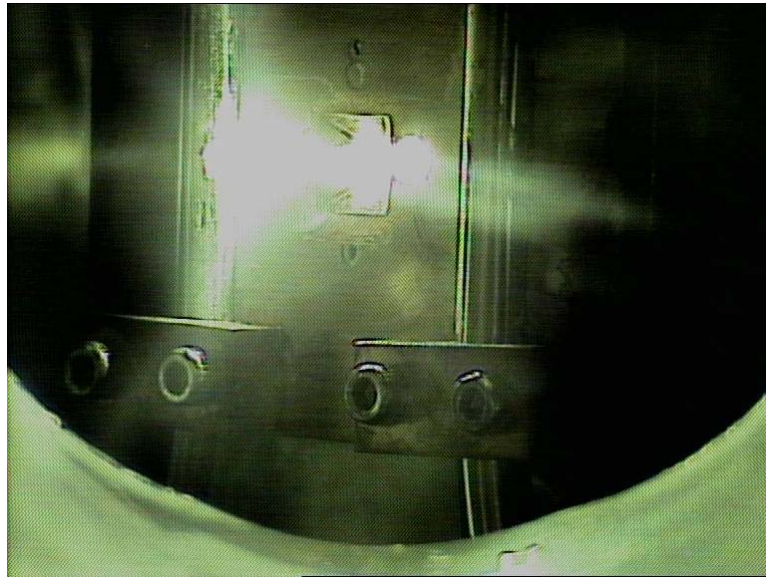


Figure 3.1 SR x-ray fan radiating on the pinhole

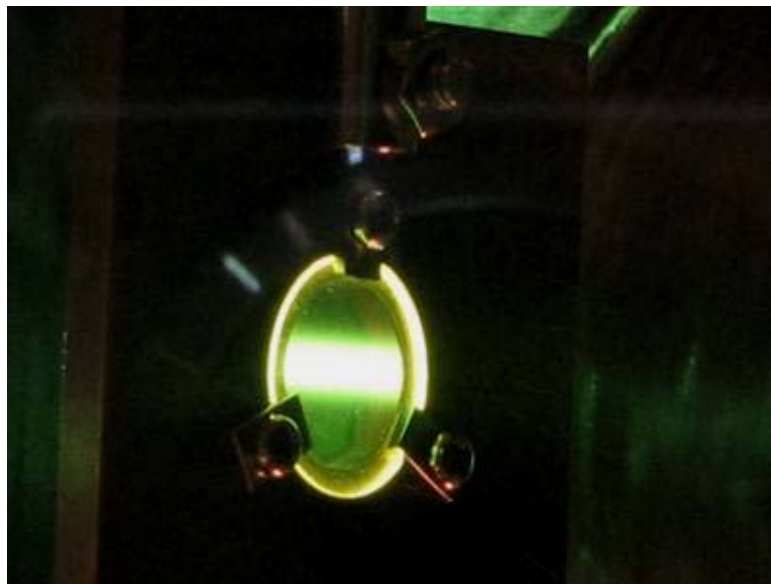


Figure 3.2 Direct x-ray fan falling on the YAG:Ce screen

When the x-ray pinhole is pulled up, the direct radiation fan will travel along the beam line. After the beamline is well aligned, when x-ray radiation fan is allowed

to hit the YAG:Ce screen, the bright strip appears. Figure 3.2 shows the direct x-ray fan falling on the fluorescent screen.

To form the x-ray image, the pinhole is pulled down to the optical axis. The fundamental geometrical optics ensures that there must be an inverted real image on the screen, if all optical components are on the optical axis. Figure 3.3 shows the x-ray beam image on the fluorescent screen after the XPI has been aligned.

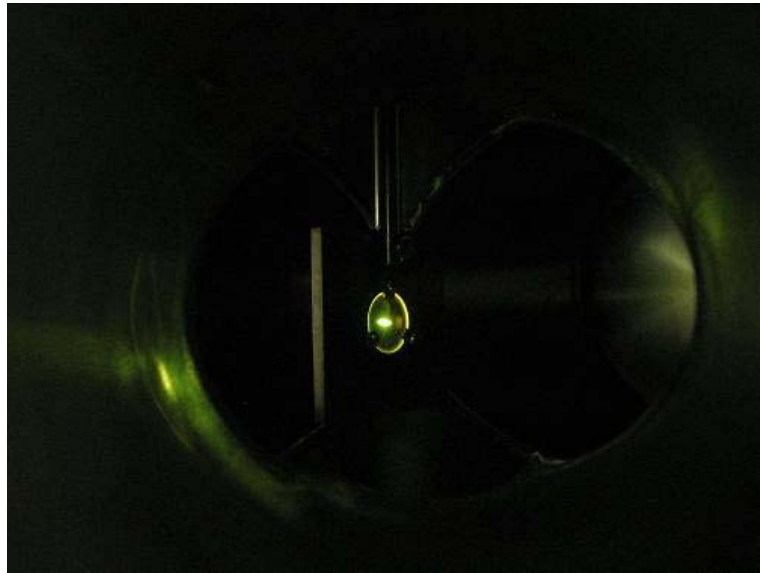


Figure 3.3 The x-ray SR beam image formed on the YAG:Ce screen

3.2 Finding the real image size

Since the x-ray beam image is taken by a CCD camera through backside observation, the real size of beam image must be calibrated. First, the pinhole image magnification factor must be known. From simple geometry, the magnification of XPI system can be determined from the distances between optical components. The distance from source to pinhole is about 2830 mm and distance from pinhole to YAG

fluorescent screen is about 4920 mm. Therefore, the magnification ratio of this XPI is about 1.74. Since the size of YAG screen opening is known, the size of beam image on the same screen could be determined. Figure 3.4 shows the x-ray beam image on the fluorescent screen viewed from back side. The real size of x-ray SR beam at source point is then calculated by dividing the image size with the magnification factor. By this way, we obtain the calibration of ratio to be approximately $27.1 \mu\text{m}$ on real image per one pixel on CCD.

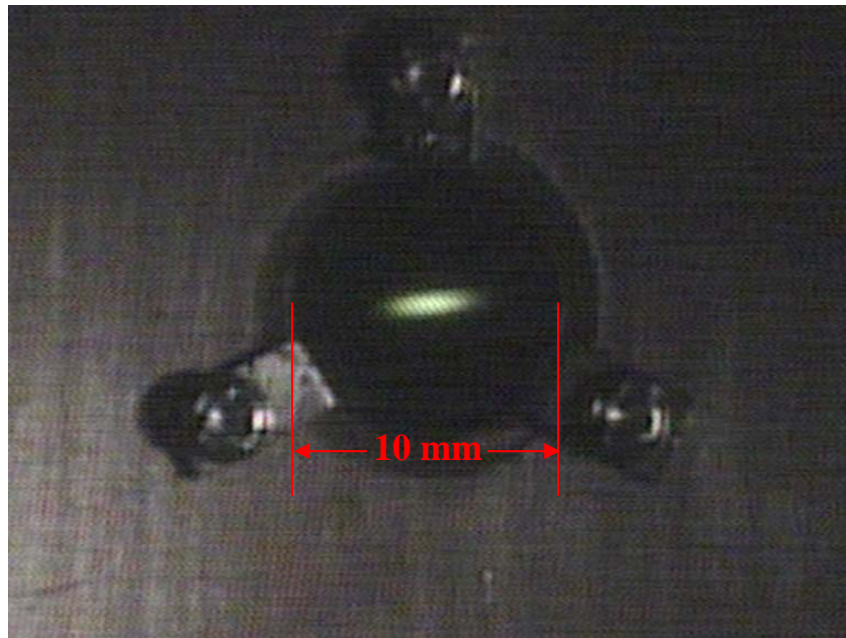


Figure 3.4 X-ray image on the YAG:Ce screen viewed from back side

3.3 Effect of pinhole aperture size

The beam size measurement may be effected by the pinhole aperture size. Smaller aperture may have a better resolution but lower visibility. Therefore, we have varied the size of pinhole aperture to be 30 μm , 50 μm and 75 μm respectively, and made the observation. The results are shown in figure 3.5. For comparison, all of the x-ray images were taken at the electron beam energy 1.2 GeV and the beam current of 90 mA. The aperture size of 75 μm was chosen since it provided better image contrast and visibility. The smaller aperture sizes gave dimmer images and higher signal to noise ratio. Note that, the pinhole with aperture size of 30 μm x 25 μm (Limborg, Safranek and Stefan, 2000) was used at SPEAR 2 for a smaller beam size compared to SPS.

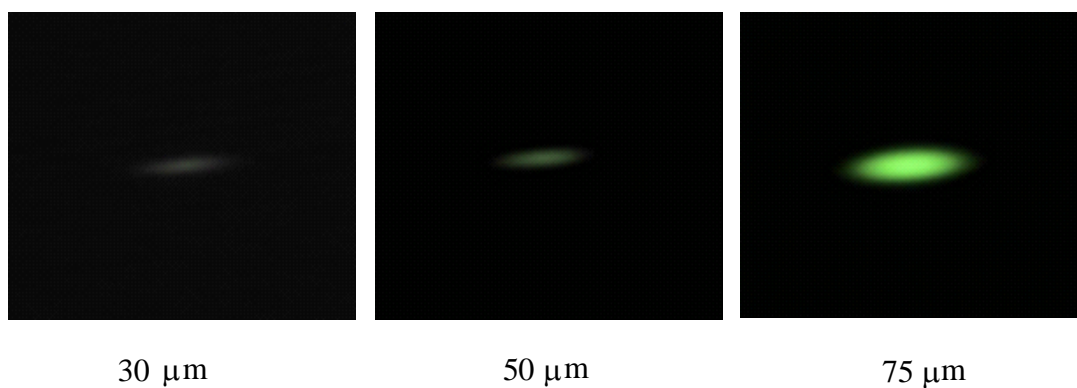


Figure 3.5 X-ray beam images taken with different pinhole aperture sizes

3.4 Beam images of different electron energy

From the synchrotron radiation spectra from SPS bending magnet as mentioned in chapter II, the electron beam at 1.2 GeV will emit more x-ray than the 1.0 GeV beam. To demonstrate this fact, the x-ray images were taken at the SPS electron beam energy of 1.0 GeV and 1.2 GeV at the beam current of about 90 mA. The results are shown in figure 3.6. Even the SR radiations in visible-UV region are quite similar, it is clear that the x-ray beam image at 1.2 GeV is much brighter than the beam image of 1.0 GeV. Note that, the effect of beam position shifted (off aligned) was not taken to consideration since the XPI was aligned for the energy 1.2 GeV.

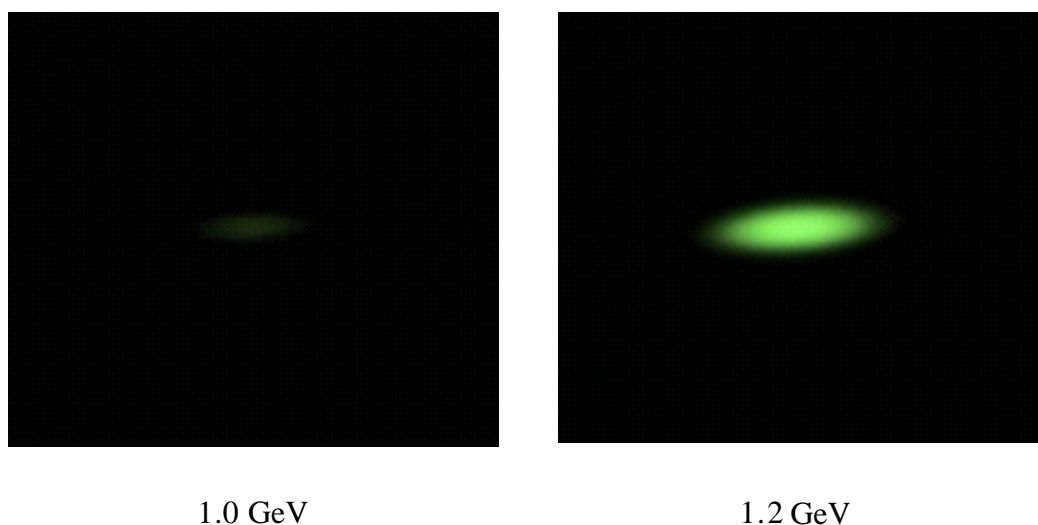


Figure 3.6 X-ray beam images for different electron beam energies

3.5 Comparison of XPI and VLI

The present design of XPI beam allows the VLI image to be taken in the same time. Therefore the quality of images taken from XPI and VLI can be compared. The result is shown in figure 3.7. It can be seen that the XPI image has better contrast and visibility, possibly due to smaller aberration in the optical system. The XPI should also have the better resolution. However, the beamsizes values measured by both techniques are quite comparable. This may be due to the fact that SPS beam is not closed to the diffraction limit yet. For smaller SR beamsizes, we believe that the XPI will out-perform the VLI system. The comparison to SRI technique could be saved for the future work.

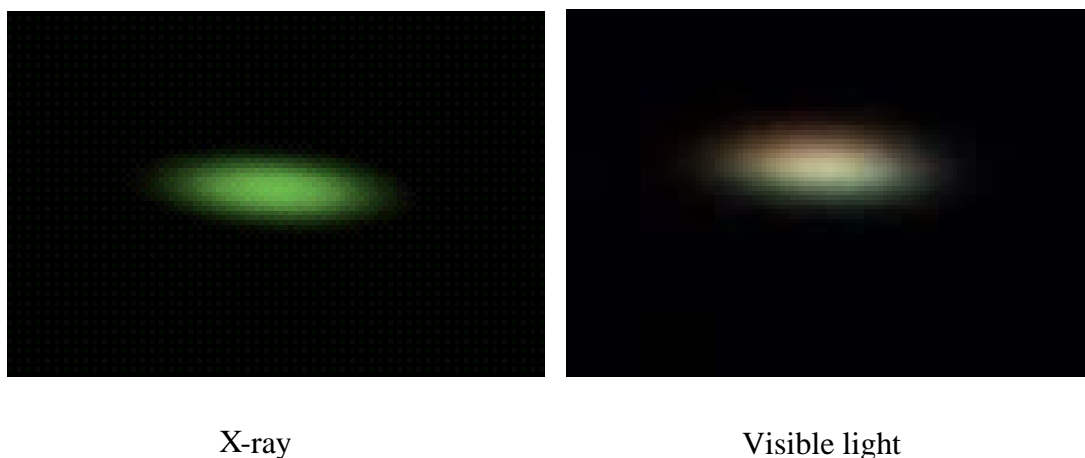


Figure 3.7 Comparison of x-ray and visible light beam images at a same condition

3.6 Finding of the natural beam size

We have measured the beam size as a function of STR current at 1.2 GeV. The data is shown in table 3.1. Both horizontal and vertical beam sizes are plot with beam current as shown in figure 3.8. The natural beam size can be obtained from the interpolated beam size at zero beam current. We have obtained the natural beam size values of SPS at 1.2 GeV to be $\sigma_{0x} = 403 \mu\text{m}$, and $\sigma_{0y} = 128 \mu\text{m}$.

Table 3.1 The SPS 1.2 GeV electron beam size at various beam currents

Beam current (mA)	σ_x (μm)	σ_y (μm)
37	560	173
38	560	173
40	570	183
41	570	173
46	601	183
50	622	183
51	612	183
55	622	194
56	632	194
60	642	204
61	662	194
65	682	214
66	682	214
70	703	204
71	713	204
75	733	214
76	723	214
80	743	214
81	743	235
85	764	224
86	774	235
90	785	235
91	785	235
95	795	245
100	815	245
101	815	245

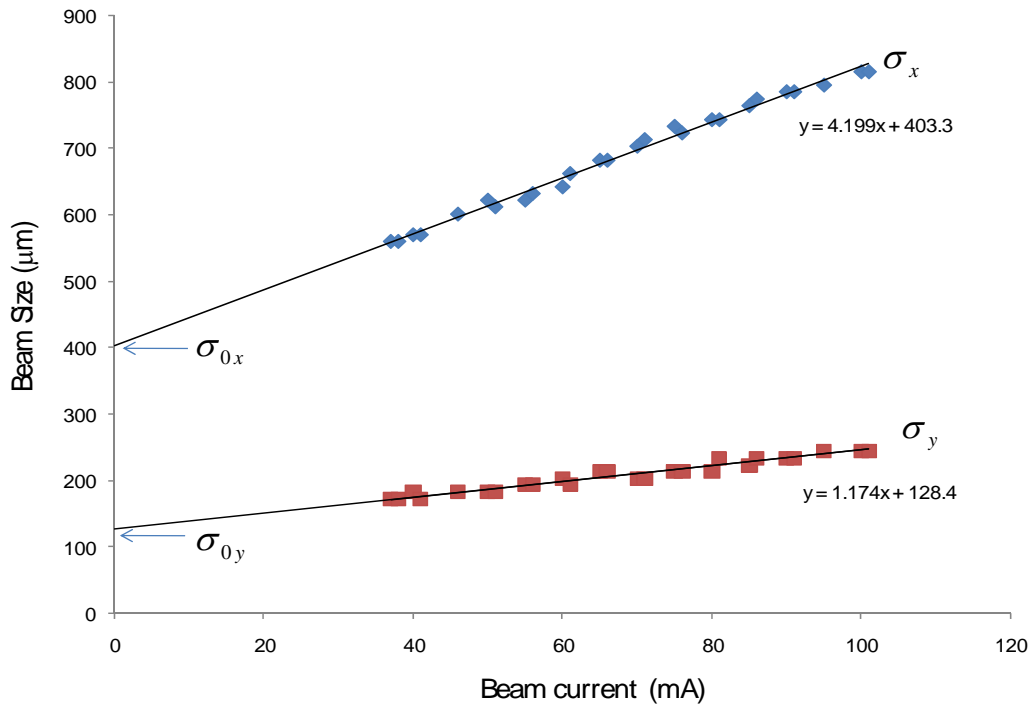


Figure 3.8 The natural beam sizes can be obtained from linear relation of beam sizes and beam current. For SPS at 1.2 GeV, $\sigma_{0x} = 403 \mu\text{m}$ and $\sigma_{0y} = 128 \mu\text{m}$.

3.7 Determination of beam emittance

The beam emittance can be estimated using the relation between beam size and betatron function at the source point. Table 3.2 shows the machine parameters used in this estimation. From equation (1.14), the horizontal beam emittance is estimated to be 83 nm rad, somewhat larger than the value of 63 nm rad predicted by the beam dynamic modeling.

Table 3.2 Machine parameters used in the determination of beam emittance

Beam parameters		
Beam emittance (model)	63	nm rad
Horizontal betatron function	1.958	m
Vertical betatron function	5.223	m
Dispersion function	0.132	m

3.8 XPI as the beam position monitor

The electron beam position can be shifted from the central orbit by changing the RF frequency as described by

$$\Delta x = \frac{\eta}{\alpha_c} \frac{\Delta f}{f_0} \quad (3.1)$$

where Δx is the shift in transverse position with respect to the center orbit, η is the dispersion function, α_c is the momentum compaction factor, Δf and f_0 are a shifted RF frequency and a normal operating RF frequency respectively. In this experiment, we demonstrated that the XPI can be used as a beam position monitor. By increasing the STR RF frequency, the electron beam orbit was shifted to the inside direction of the ring as shown in figure 3.9.

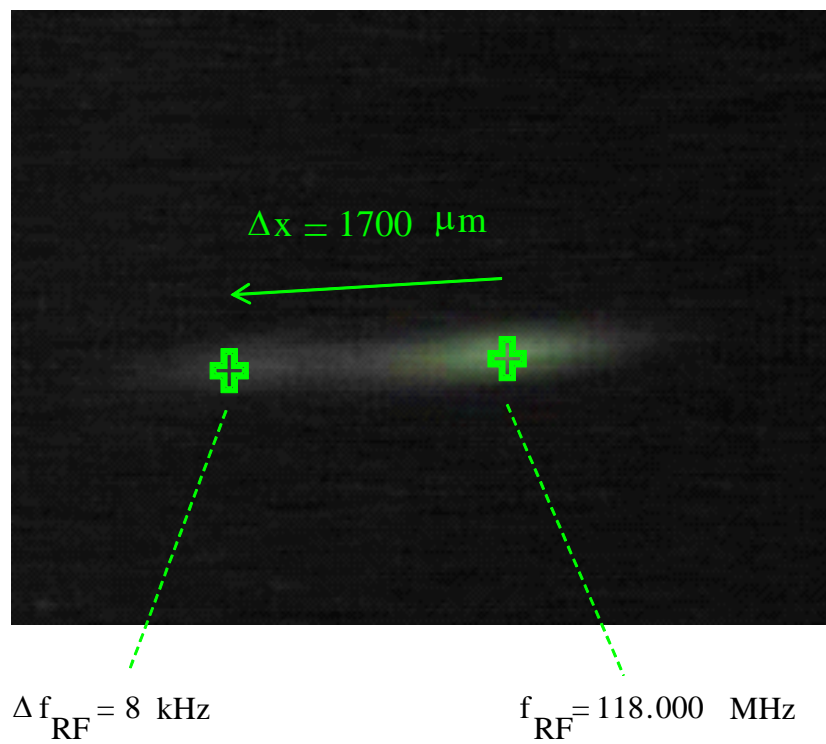


Figure 3.9 Electron beam position shifted cause by changing the RF frequency

CHAPTER IV

CONCLUSIONS

In this thesis, we have described the design and construction of the x-ray pinhole imaging system for beam diagnostic purpose at the Siam Photon Laboratory. The working principle of XPI is similar to that of a pinhole camera. The difference is XPI uses x-ray instead of visible light.

Most of the components of XPI system were constructed using NSRC in-house technology. The NSRC built vacuum chambers have achieved the UHV level. The machine control and image processing system for XPI were developed in-house. In general, the NSRC-built system has operated at the level up to the expectation.

The x-ray pinhole is the main component developed in this work. The tantalum pinhole with adjustable aperture size was fabricated and tested. The pinhole was used successfully in projection of the x-ray image onto the fluorescent screen. The electron beam size of SPS storage ring was obtained from x-ray beam image analysis. The measured horizontal natural beam size was 403 μm , and the measured vertical beam size was 128 μm for the 1.2 GeV SPS storage ring. The horizontal beam emittance was determined to be 83 nm rad higher than the theoretical value of 63 nm rad. The discrepancy may be arisen from many effects such as beam instability, machine misalignment or inaccurate value of betatron functions. Those effects may be the topics for future study.

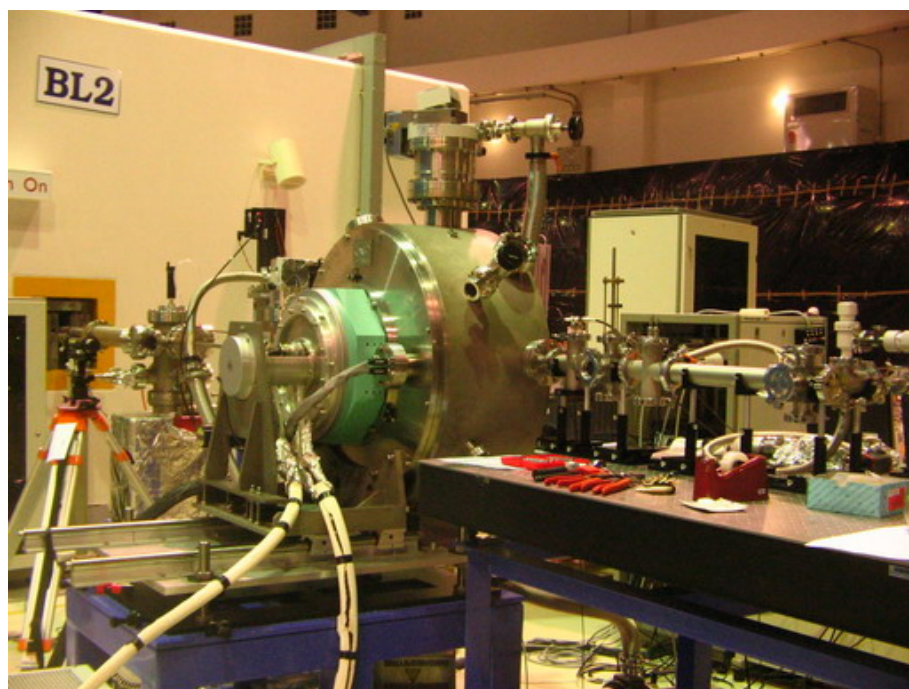


Figure 4.1 The new x-ray beamline at BL2 built by sharing the vacuum system with the XPI project

REFERENCES

REFERENCES

- Berg, W.J. et al. (2000). Characterization of Ce-doped scintillating crystals for imaging electron beams at APS linac. **Linac Conference 2000**. Monterey.
- Chevtsov, P. et al. (2003). Synchrotron interferometer at Jefferson lab. **PAC 2003**. Portland.
- Duke, P.J. (2000). **Synchrotron radiation production and properties**. USA: Oxford university press .
- Graves, W.S and Johnson, E.D.(1997). A high resolution electron beam profile monitor, **PAC 1997**. Vancouver.
- Hecht, E (2001). **Optics** (4th ed). USA: Adison Wesley.
- Kaczmarek, S.M et al. (1999). Changes in optical properties of Ce:YAG crystals under annealing and irradiation processing. **Crystal Research and Technology**, 34(8): 1013-1036.
- Kawkasem, C. (2007). Design parameters for the low emittance mode at 1.2 GeV SPS storage ring. **NSRC Technical Note**. Nakhon Ratchasima.
- Kawkasem, C. (2007). Measurement of the betatron functions for the beam service configuration at 1.2 GeV. **NSRC Technical Note**. Nakhon Ratchasima.
- Kawkasem, C. (2007). Measurement of the dispersion function for the beam service configuration at 1.2 GeV. **NSRC Technical Note**. Nakhon Ratchasima.
- Kunz, C. (1979). **Synchrotron radiation techniques and applications**. USA: Spriger.

- Limborg, C. et al. (2002). A pinhole camera for SPEAR2. **SLAC-PUB-9462**.
- Masaki, M., and Takano, S. (2001). Beam size measurement of the Spring 8 storage ring by two-dimensional interferometer. **DIPAC 2001**. Grenoble.
- Mitsuhashi, T. et al. (1999). Measurement of small beam size by the use of SR interferometer. **PAC 1999**. New York.
- Safranek, J., and Stefan, P.M. (1996). Emittance measurement at the NSLS X-ray ring. **EPAC 1996**. Sitge.
- Sannibale, F et al. (2003). A second beam-diagnostic beamline for the Advanced Light Source. **PAC 2003**. Portland.
- Takayama, Y. et al. (1999). Application limit of SR interferometer for emittance measurement. **PAC 1999**. New York.
- Turner, S. (1998). **Synchrotron radiation and free electron laser**. CERN Accelerator school.
- Turner, S. (1999). **Vacuum technology**. CERN Accelerator School.
- Wiedemann, H. (2002). **Synchrotron radiation**. USA: Springer.
- Wiedemann, H. (1999). **Particle Accelerator Physics I** (2nd ed). USA: Springer.
- Wiedemann, H. (1999). **Particle Accelerator Physics II** (2nd ed). USA: Springer.

APPENDICES

APPENDIX A

RESULTS FROM BEAM OPTICS CALCULATION

A1. Initial beam parameters

Beam parameter

Particle Type	electron	
Rest mass mc^2	511.003	keV
init.kinetic Energy, E_{kin}	1.199	GeV
init.particle momentum, cp	1.200	GeV
init.relativistic factor, γ	2348.321	
int.particle velocity, v/c	1	
norm.emittance, $\epsilonps_x \cdot \gamma$	23483.212	mm*mrad
norm emittance, $\epsilonps_y \cdot \gamma$	23483.212	mm*mrad

A2. Beam parameters list

Name	betax(m)	alphax	dnuex	etax(m)	etap(mr)	betay(m)	alphay	dnu ey	s(m)
Start	15.247	0	0	0.355	0	3.403	0	0	0
d1	15.896	-0.206	0.032	0.355	0	6.308	-0.924	0.119	3.144
sth1	15.896	-0.206	0.032	0.355	0	6.308	-0.924	0.119	3.144
d2	15.967	-0.217	0.034	0.355	0	6.626	-0.973	0.123	3.312
esm1	15.967	-0.217	0.034	0.355	0	6.626	-0.973	0.123	3.312
d3	16.043	-0.228	0.036	0.355	0	6.969	-1.024	0.127	3.484
qf11	12.392	10.548	0.039	0.31	-0.271	9.732	-8.253	0.133	3.807
d4	8.942	8.944	0.042	0.263	-0.271	12.876	-9.509	0.136	3.984
stv1	8.942	8.944	0.042	0.263	-0.271	12.876	-9.509	0.136	3.984
d5	5.87	7.223	0.046	0.211	-0.271	16.746	10.859	0.138	4.174
qd21	3.095	2.136	0.059	0.149	-0.122	19.056	4.37	0.141	4.497
d6	1.707	1.438	0.086	0.102	-0.122	15.82	3.96	0.144	4.885
bm01	1.105	1.035	0.114	0.083	-0.037	13.96	3.704	0.147	5.128
bm01	0.707	0.602	0.158	0.084	0.048	12.225	3.449	0.15	5.37
bm01	0.524	0.15	0.223	0.106	0.132	10.614	3.193	0.153	5.613
bm01	0.563	-0.307	0.297	0.148	0.215	9.127	2.937	0.157	5.855
bm01	0.821	-0.754	0.355	0.21	0.297	7.764	2.681	0.162	6.098

A2. Beam parameters list (Continued)

Name	betax(m)	alphax	dnuey	etax(m)	etap(mr)	betay(m)	alphay	dnuey	s(m)
bm01	1.291	-1.178	0.393	0.292	0.376	6.525	2.425	0.167	6.341
bm01	1.958	-1.567	0.417	0.392	0.453	5.41	2.169	0.174	6.583
bm01	2.803	-1.908	0.434	0.511	0.526	4.42	1.913	0.182	6.826
bm01	3.8	-2.19	0.445	0.647	0.595	3.554	1.658	0.191	7.068
d7	6.138	-2.89	0.461	0.921	0.595	2.252	1.172	0.217	7.528
esm2	6.138	-2.89	0.461	0.921	0.595	2.252	1.172	0.217	7.528
d8	6.876	-3.08	0.464	0.995	0.595	1.978	1.042	0.227	7.652
qf31	7.176	2.227	0.471	1.062	-0.19	1.828	-0.54	0.255	7.975
d9	6.734	2.143	0.473	1.042	-0.19	1.944	-0.611	0.263	8.076
sf	6.01	1.998	0.477	1.009	-0.19	2.18	-0.735	0.277	8.251
d10	5.544	1.899	0.481	0.987	-0.19	2.365	-0.819	0.285	8.37
sth2	5.544	1.899	0.481	0.987	-0.19	2.365	-0.819	0.285	8.37
d11	2.135	0.88	0.539	0.754	-0.19	5.44	-1.686	0.341	9.597
esm3	2.135	0.88	0.539	0.754	-0.19	5.44	-1.686	0.341	9.597
d12	2.004	0.815	0.545	0.739	-0.19	5.706	-1.741	0.343	9.675
sd	1.679	0.628	0.564	0.697	-0.19	6.525	-1.9	0.349	9.9
d9	1.561	0.544	0.574	0.678	-0.19	6.916	-1.972	0.351	10
qd41	1.561	-0.54	0.608	0.678	0.189	6.916	1.972	0.359	10.32
d9	1.679	-0.63	0.618	0.697	0.189	6.525	1.9	0.361	10.43
sd	2.004	-0.82	0.638	0.739	0.189	5.706	1.741	0.367	10.65
d13	2.173	-0.9	0.645	0.758	0.189	5.368	1.671	0.37	10.75
stv2	2.173	-0.9	0.645	0.758	0.189	5.368	1.671	0.37	10.75
d14	5.544	-1.9	0.702	0.987	0.189	2.365	0.819	0.425	11.95
sth3	5.544	-1.9	0.702	0.987	0.189	2.365	0.819	0.425	11.95
d10	6.01	-2	0.705	1.009	0.189	2.18	0.735	0.433	12.07
sf	6.735	-2.14	0.71	1.042	0.189	1.944	0.611	0.447	12.25
d9	7.176	-2.23	0.712	1.061	0.189	1.828	0.54	0.455	12.35
qf32	6.876	3.081	0.719	0.995	-0.595	1.978	-1.042	0.483	12.67
d8	6.138	2.892	0.722	0.921	-0.595	2.252	-1.172	0.493	12.8
esm4	6.138	2.892	0.722	0.921	-0.595	2.252	-1.172	0.493	12.8
d7	3.8	2.19	0.737	0.647	-0.595	3.554	-1.658	0.519	13.26
bm02	2.803	1.908	0.749	0.511	-0.526	4.42	-1.913	0.528	13.5
bm02	1.958	1.567	0.765	0.392	-0.453	5.41	-2.169	0.536	13.74
bm02	1.291	1.178	0.79	0.292	-0.376	6.525	-2.425	0.543	13.98
bm02	0.821	0.754	0.828	0.21	-0.297	7.764	-2.681	0.548	14.23
bm02	0.563	0.307	0.886	0.148	-0.215	9.127	-2.937	0.553	14.47
bm02	0.524	-0.15	0.959	0.106	-0.132	10.614	-3.193	0.557	14.71
bm02	0.707	-0.6	1.024	0.084	-0.048	12.225	-3.449	0.56	14.96
bm02	1.105	-1.04	1.069	0.083	0.037	13.96	-3.704	0.563	15.2
bm02	1.707	-1.44	1.097	0.102	0.122	15.82	-3.96	0.566	15.44
d6	3.095	-2.14	1.124	0.149	0.122	19.056	-4.37	0.569	15.83
qd22	5.87	-7.22	1.136	0.211	0.271	16.746	10.859	0.572	16.15
d5	8.942	-8.94	1.141	0.263	0.271	12.876	9.509	0.574	16.34
stv3	8.942	-8.94	1.141	0.263	0.271	12.876	9.509	0.574	16.34
d4	12.392	-10.5	1.143	0.31	0.271	9.732	8.253	0.577	16.52
qf12	16.043	0.228	1.147	0.355	0	6.969	1.024	0.583	16.84
d3	15.967	0.217	1.148	0.355	0	6.626	0.973	0.587	17.01

A2. Beam parameters list (Continued)

Name	betax(m)	alphax	dnuey	etax(m)	etap(mr)	betay(m)	alphay	dnuey	s(m)
esm5	15.967	0.217	1.148	0.355	0	6.626	0.973	0.587	17.01
d2	15.896	0.206	1.15	0.355	0	6.308	0.924	0.591	17.18
sth4	15.896	0.206	1.15	0.355	0	6.308	0.924	0.591	17.18
d1	15.247	0	1.183	0.355	0	3.403	0	0.71	20.33
d1	15.896	-0.21	1.215	0.355	0	6.308	-0.924	0.829	23.47
sth5	15.896	-0.21	1.215	0.355	0	6.308	-0.924	0.829	23.47
d2	15.967	-0.22	1.217	0.355	0	6.626	-0.973	0.833	23.64
esm6	15.967	-0.22	1.217	0.355	0	6.626	-0.973	0.833	23.64
d3	16.043	-0.23	1.218	0.355	0	6.969	-1.024	0.837	23.81
qf13	12.392	10.55	1.222	0.31	-0.271	9.732	-8.253	0.843	24.13
d4	8.942	8.945	1.224	0.263	-0.271	12.876	-9.509	0.846	24.31
stv4	8.942	8.945	1.224	0.263	-0.271	12.876	-9.509	0.846	24.31
d5	5.87	7.223	1.229	0.211	-0.271	16.746	-10.85	0.848	24.5
qd23	3.095	2.136	1.241	0.149	-0.122	19.056	4.37	0.851	24.82
d6	1.707	1.438	1.268	0.102	-0.122	15.82	3.96	0.854	25.21
bm03	1.105	1.035	1.296	0.083	-0.037	13.96	3.704	0.857	25.45
bm03	0.707	0.602	1.341	0.084	0.048	12.225	3.449	0.86	25.7
bm03	0.524	0.15	1.406	0.106	0.132	10.614	3.193	0.863	25.94
bm03	0.563	-0.31	1.479	0.148	0.215	9.127	2.937	0.867	26.18
bm03	0.821	-0.75	1.537	0.21	0.297	7.764	2.681	0.872	26.42
bm03	1.291	-1.18	1.575	0.292	0.376	6.525	2.425	0.877	26.67
bm03	1.958	-1.57	1.6	0.392	0.453	5.41	2.169	0.884	26.91
bm03	2.803	-1.91	1.616	0.511	0.526	4.42	1.913	0.892	27.15
bm03	3.8	-2.19	1.628	0.647	0.595	3.554	1.658	0.901	27.39
d7	6.138	-2.89	1.643	0.921	0.595	2.252	1.172	0.927	27.85
esm7	6.138	-2.89	1.643	0.921	0.595	2.252	1.172	0.927	27.85
d8	6.876	-3.08	1.646	0.995	0.595	1.978	1.042	0.937	27.98
qf33	7.176	2.227	1.653	1.061	-0.189	1.828	-0.54	0.965	28.3
d9	6.734	2.143	1.655	1.042	-0.189	1.944	-0.611	0.973	28.4
sf	6.01	1.998	1.66	1.009	-0.189	2.18	-0.735	0.987	28.58
d10	5.544	1.899	1.663	0.987	-0.189	2.365	-0.819	0.995	28.7
sth6	5.544	1.899	1.663	0.987	-0.189	2.365	-0.819	0.995	28.7
d14	2.173	0.897	1.72	0.758	-0.189	5.368	-1.671	1.05	29.9
stv5	2.173	0.897	1.72	0.758	-0.189	5.368	-1.671	1.05	29.9
d13	2.004	0.815	1.727	0.739	-0.189	5.706	-1.741	1.053	30
sd	1.679	0.628	1.747	0.697	-0.189	6.525	-1.9	1.059	30.23
d9	1.561	0.544	1.757	0.678	-0.189	6.916	-1.972	1.061	30.33
qd42	1.561	-0.54	1.791	0.678	0.19	6.916	1.972	1.069	30.65
d9	1.679	-0.63	1.801	0.697	0.19	6.525	1.9	1.071	30.75
sd	2.004	-0.82	1.82	0.739	0.19	5.706	1.741	1.077	30.98
d12	2.135	-0.88	1.826	0.754	0.19	5.44	1.686	1.079	31.05
esm8	2.135	-0.88	1.826	0.754	0.19	5.44	1.686	1.079	31.05
d11	5.544	-1.9	1.884	0.987	0.19	2.365	0.819	1.135	32.28
sth7	5.544	-1.9	1.884	0.987	0.19	2.365	0.819	1.135	32.28
d10	6.01	-2	1.888	1.009	0.19	2.18	0.735	1.143	32.4
sf	6.735	-2.14	1.892	1.042	0.19	1.944	0.611	1.157	32.57
d9	7.176	-2.23	1.894	1.062	0.19	1.828	0.54	1.165	32.68
sd	2.004	-0.82	1.82	0.739	0.19	5.706	1.741	1.077	30.98

A2. Beam parameter lists (Continued)

Name	betax(m)	alphax	dnuey	etax(m)	etap(mr)	betay(m)	alphay	dnuey	s(m)
d12	2.135	-0.88	1.826	0.754	0.19	5.44	1.686	1.079	31.05
esm8	2.135	-0.88	1.826	0.754	0.19	5.44	1.686	1.079	31.05
d11	5.544	-1.9	1.884	0.987	0.19	2.365	0.819	1.135	32.28
sth7	5.544	-1.9	1.884	0.987	0.19	2.365	0.819	1.135	32.28
d10	6.01	-2	1.888	1.009	0.19	2.18	0.735	1.143	32.4
sf	6.735	-2.14	1.892	1.042	0.19	1.944	0.611	1.157	32.57
d9	7.176	-2.23	1.894	1.062	0.19	1.828	0.54	1.165	32.68
qf34	6.876	3.081	1.901	0.995	-0.595	1.978	-1.042	1.193	33
d8	6.138	2.892	1.904	0.921	-0.595	2.252	-1.172	1.203	33.12
esm9	6.138	2.892	1.904	0.921	-0.595	2.252	-1.172	1.203	33.12
d7	3.8	2.19	1.92	0.647	-0.595	3.554	-1.658	1.229	33.58
bm04	2.803	1.908	1.931	0.511	-0.526	4.42	-1.913	1.238	33.82
bm04	1.958	1.567	1.948	0.392	-0.453	5.41	-2.169	1.246	34.07
bm04	1.291	1.178	1.972	0.292	-0.376	6.525	-2.425	1.253	34.31
bm04	0.821	0.754	2.01	0.21	-0.297	7.764	-2.681	1.258	34.55
bm04	0.563	0.307	2.068	0.148	-0.215	9.127	-2.937	1.263	34.79
bm04	0.524	-0.15	2.142	0.106	-0.132	10.614	-3.193	1.267	35.04
bm04	0.707	-0.6	2.207	0.084	-0.048	12.225	-3.449	1.27	35.28
bm04	1.105	-1.04	2.251	0.083	0.037	13.96	-3.704	1.273	35.52
bm04	1.707	-1.44	2.279	0.102	0.122	15.82	-3.96	1.276	35.77
d6	3.095	-2.14	2.306	0.149	0.122	19.056	-4.37	1.279	36.15
qd24	5.87	-7.22	2.319	0.211	0.27	16.746	10.859	1.282	36.48
d5	8.942	-8.94	2.323	0.262	0.27	12.876	9.509	1.284	36.67
stv6	8.942	-8.94	2.323	0.262	0.27	12.876	9.509	1.284	36.67
d4	12.392	-10.5	2.326	0.31	0.27	9.732	8.253	1.287	36.84
qf14	16.043	0.228	2.329	0.355	0	6.969	1.024	1.293	37.17
d3	15.967	0.217	2.331	0.355	0	6.626	0.973	1.297	37.34
es10	15.967	0.217	2.331	0.355	0	6.626	0.973	1.297	37.34
d2	15.896	0.206	2.333	0.355	0	6.308	0.924	1.301	37.51
sth8	15.896	0.206	2.333	0.355	0	6.308	0.924	1.301	37.51
d1	15.247	0	2.365	0.355	0	3.403	0	1.42	40.65
d1	15.896	-0.21	2.397	0.355	0	6.308	-0.924	1.539	43.79
sth9	15.896	-0.21	2.397	0.355	0	6.308	-0.924	1.539	43.79
d2	15.967	-0.22	2.399	0.355	0	6.626	-0.973	1.543	43.96
es11	15.967	-0.22	2.399	0.355	0	6.626	-0.973	1.543	43.96
d3	16.043	-0.23	2.401	0.355	0	6.969	-1.024	1.547	44.13
qf15	12.392	10.55	2.404	0.31	-0.27	9.732	-8.253	1.553	44.46
d4	8.942	8.944	2.407	0.262	-0.27	12.876	-9.509	1.556	44.63
stv7	8.942	8.944	2.407	0.262	-0.27	12.876	-9.509	1.556	44.63
d5	5.87	7.223	2.411	0.211	-0.27	16.746	-10.85	1.558	44.82
qd25	3.095	2.136	2.424	0.149	-0.122	19.056	4.37	1.561	45.15
d6	1.707	1.438	2.451	0.102	-0.122	15.82	3.96	1.564	45.54
bm05	1.105	1.035	2.479	0.083	-0.037	13.96	3.704	1.567	45.78
bm05	0.707	0.602	2.523	0.084	0.048	12.225	3.449	1.57	46.02
bm05	0.524	0.15	2.588	0.106	0.132	10.614	3.193	1.573	46.26
bm05	0.563	-0.31	2.662	0.148	0.215	9.127	2.937	1.577	46.51
bm05	0.821	-0.75	2.72	0.21	0.297	7.764	2.681	1.582	46.75

A2. Beam parameters list (Continued)

Name	betax(m)	alphax	dnuey	etax(m)	etap(mr)	betay(m)	alphay	dnuey	s(m)
bm05	1.291	-1.18	2.758	0.292	0.376	6.525	2.425	1.587	46.99
bm05	1.958	-1.57	2.782	0.392	0.453	5.41	2.169	1.594	47.23
bm05	2.803	-1.91	2.799	0.511	0.526	4.42	1.913	1.602	47.48
bm05	3.8	-2.19	2.81	0.647	0.595	3.554	1.658	1.611	47.72
d7	6.138	-2.89	2.826	0.921	0.595	2.252	1.172	1.637	48.18
es12	6.138	-2.89	2.826	0.921	0.595	2.252	1.172	1.637	48.18
d8	6.876	-3.08	2.829	0.995	0.595	1.978	1.042	1.647	48.3
qf35	7.176	2.227	2.836	1.062	-0.19	1.828	-0.54	1.675	48.63
d9	6.734	2.143	2.838	1.042	-0.19	1.944	-0.611	1.683	48.73
sf	6.01	1.998	2.842	1.009	-0.19	2.18	-0.735	1.697	48.9
d10	5.544	1.899	2.846	0.987	-0.19	2.365	-0.819	1.705	49.02
sh10	5.544	1.899	2.846	0.987	-0.19	2.365	-0.819	1.705	49.02
d11	2.135	0.88	2.904	0.754	-0.19	5.44	-1.686	1.761	50.25
es13	2.135	0.88	2.904	0.754	-0.19	5.44	-1.686	1.761	50.25
d12	2.004	0.815	2.91	0.739	-0.19	5.706	-1.741	1.763	50.33
sd	1.679	0.628	2.929	0.697	-0.19	6.525	-1.9	1.769	50.55
d9	1.561	0.544	2.939	0.678	-0.19	6.916	-1.972	1.771	50.65
qd43	1.561	-0.54	2.973	0.678	0.19	6.916	1.972	1.779	50.97
d9	1.679	-0.63	2.983	0.697	0.19	6.525	1.9	1.781	51.08
sd	2.004	-0.82	3.003	0.739	0.19	5.706	1.741	1.787	51.3
d13	2.173	-0.9	3.01	0.758	0.19	5.368	1.671	1.79	51.4
stv8	2.173	-0.9	3.01	0.758	0.19	5.368	1.671	1.79	51.4
d14	5.544	-1.9	3.067	0.987	0.19	2.365	0.819	1.845	52.6
sth3	5.544	-1.9	3.067	0.987	0.19	2.365	0.819	1.845	52.6
d10	6.01	-2	3.07	1.009	0.19	2.18	0.735	1.853	52.72
sf	6.735	-2.14	3.075	1.042	0.19	1.944	0.611	1.867	52.9
d9	7.176	-2.23	3.077	1.062	0.19	1.828	0.54	1.875	53
qf36	6.876	3.081	3.084	0.995	-0.595	1.978	-1.042	1.903	53.32
d8	6.138	2.892	3.087	0.921	-0.595	2.252	-1.172	1.913	53.45
es14	6.138	2.892	3.087	0.921	-0.595	2.252	-1.172	1.913	53.45
d7	3.8	2.19	3.102	0.647	-0.595	3.554	-1.658	1.939	53.91
bm06	2.803	1.908	3.114	0.511	-0.526	4.42	-1.913	1.948	54.15
bm06	1.958	1.567	3.13	0.392	-0.453	5.41	-2.169	1.956	54.39
bm06	1.291	1.178	3.155	0.292	-0.376	6.525	-2.425	1.963	54.63
bm06	0.821	0.754	3.193	0.21	-0.297	7.764	-2.681	1.968	54.88
bm06	0.563	0.307	3.251	0.148	-0.215	9.127	-2.937	1.973	55.12
bm06	0.524	-0.15	3.324	0.106	-0.132	10.614	-3.193	1.977	55.36
bm06	0.707	-0.6	3.389	0.084	-0.048	12.225	-3.449	1.98	55.6
bm06	1.105	-1.04	3.434	0.083	0.037	13.96	-3.704	1.983	55.85
bm06	1.707	-1.44	3.462	0.102	0.122	15.82	-3.96	1.986	56.09
d6	3.095	-2.14	3.489	0.149	0.122	19.056	-4.37	1.989	56.48
qd26	5.87	-7.22	3.501	0.211	0.27	16.746	10.859	1.992	56.8
d5	8.942	-8.95	3.506	0.262	0.27	12.876	9.509	1.994	56.99
stv9	8.942	-8.95	3.506	0.262	0.27	12.876	9.509	1.994	56.99
d4	12.392	-10.5	3.508	0.31	0.27	9.732	8.253	1.997	57.17
qf16	16.043	0.228	3.512	0.355	0	6.969	1.024	2.003	57.49
d3	15.967	0.217	3.513	0.355	0	6.626	0.973	2.007	57.66
es15	15.967	0.217	3.513	0.355	0	6.626	0.973	2.007	57.66

A2. Beam parameters list (Continued)

Name	betax(m)	alphax	dnuey	etax(m)	etap(mr)	betay(m)	alphay	dnuey	s(m)
d2	15.896	0.206	3.515	0.355	0	6.308	0.924	2.011	57.83
sh12	15.896	0.206	3.515	0.355	0	6.308	0.924	2.011	57.83
d1	15.247	0	3.547	0.355	0	3.403	0	2.13	60.97
d1	15.896	-0.21	3.58	0.355	0	6.308	-0.924	2.249	64.12
sh13	15.896	-0.21	3.58	0.355	0	6.308	-0.924	2.249	64.12
d2	15.967	-0.22	3.582	0.355	0	6.626	-0.973	2.253	64.29
es16	15.967	-0.22	3.582	0.355	0	6.626	-0.973	2.253	64.29
d3	16.043	-0.23	3.583	0.355	0	6.969	-1.024	2.257	64.46
qf17	12.392	10.55	3.587	0.31	-0.27	9.732	-8.253	2.263	64.78
d4	8.942	8.945	3.589	0.262	-0.27	12.876	-9.509	2.266	64.96
sv10	8.942	8.945	3.589	0.262	-0.27	12.876	-9.509	2.266	64.96
d5	5.87	7.223	3.594	0.211	-0.27	16.746	-10.85	2.268	65.15
qd27	3.095	2.136	3.606	0.149	-0.122	19.056	4.37	2.271	65.47
d6	1.707	1.438	3.633	0.102	-0.122	15.82	3.96	2.274	65.86
bm07	1.105	1.035	3.661	0.083	-0.037	13.96	3.704	2.277	66.1
bm07	0.707	0.602	3.706	0.084	0.048	12.225	3.449	2.28	66.35
bm07	0.524	0.15	3.771	0.106	0.132	10.614	3.193	2.283	66.59
bm07	0.563	-0.31	3.844	0.148	0.215	9.127	2.937	2.287	66.83
bm07	0.821	-0.75	3.902	0.21	0.297	7.764	2.681	2.292	67.07
bm07	1.291	-1.18	3.94	0.292	0.376	6.525	2.425	2.297	67.32
bm07	1.958	-1.57	3.965	0.392	0.453	5.41	2.169	2.304	67.56
bm07	2.803	-1.91	3.981	0.511	0.526	4.42	1.913	2.312	67.8
bm07	3.8	-2.19	3.993	0.647	0.595	3.554	1.658	2.321	68.04
d7	6.138	-2.89	4.008	0.921	0.595	2.252	1.172	2.347	68.5
es17	6.138	-2.89	4.008	0.921	0.595	2.252	1.172	2.347	68.5
d8	6.876	-3.08	4.011	0.995	0.595	1.978	1.042	2.357	68.63
qf37	7.176	2.227	4.018	1.062	-0.19	1.828	-0.54	2.385	68.95
d9	6.735	2.143	4.02	1.042	-0.19	1.944	-0.611	2.393	69.05
sf	6.01	1.998	4.025	1.009	-0.19	2.18	-0.735	2.407	69.23
d10	5.544	1.899	4.028	0.987	-0.19	2.365	-0.819	2.415	69.35
sh14	5.544	1.899	4.028	0.987	-0.19	2.365	-0.819	2.415	69.35
d14	2.173	0.897	4.085	0.758	-0.19	5.368	-1.671	2.47	70.55
sv11	2.173	0.897	4.085	0.758	-0.19	5.368	-1.671	2.47	70.55
d13	2.004	0.815	4.092	0.739	-0.19	5.706	-1.741	2.473	70.65
sd	1.679	0.628	4.112	0.697	-0.19	6.525	-1.9	2.479	70.87
d9	1.561	0.544	4.122	0.678	-0.19	6.916	-1.972	2.481	70.98
qd44	1.561	-0.54	4.156	0.678	0.189	6.916	1.972	2.489	71.3
d9	1.679	-0.63	4.166	0.697	0.189	6.525	1.9	2.491	71.4
sd	2.004	-0.82	4.185	0.739	0.189	5.706	1.741	2.497	71.62
d12	2.135	-0.88	4.191	0.754	0.189	5.44	1.686	2.499	71.7
es18	2.135	-0.88	4.191	0.754	0.189	5.44	1.686	2.499	71.7
d11	5.544	-1.9	4.249	0.987	0.189	2.365	0.819	2.555	72.93
sh15	5.544	-1.9	4.249	0.987	0.189	2.365	0.819	2.555	72.93
d10	6.01	-2	4.253	1.009	0.189	2.18	0.735	2.563	73.05
sf	6.734	-2.14	4.257	1.042	0.189	1.944	0.611	2.577	73.22
d9	7.176	-2.23	4.259	1.062	0.189	1.828	0.54	2.585	73.32
qf38	6.876	3.081	4.266	0.995	-0.595	1.978	-1.042	2.613	73.65
d8	6.138	2.892	4.269	0.921	-0.595	2.252	-1.172	2.623	73.77

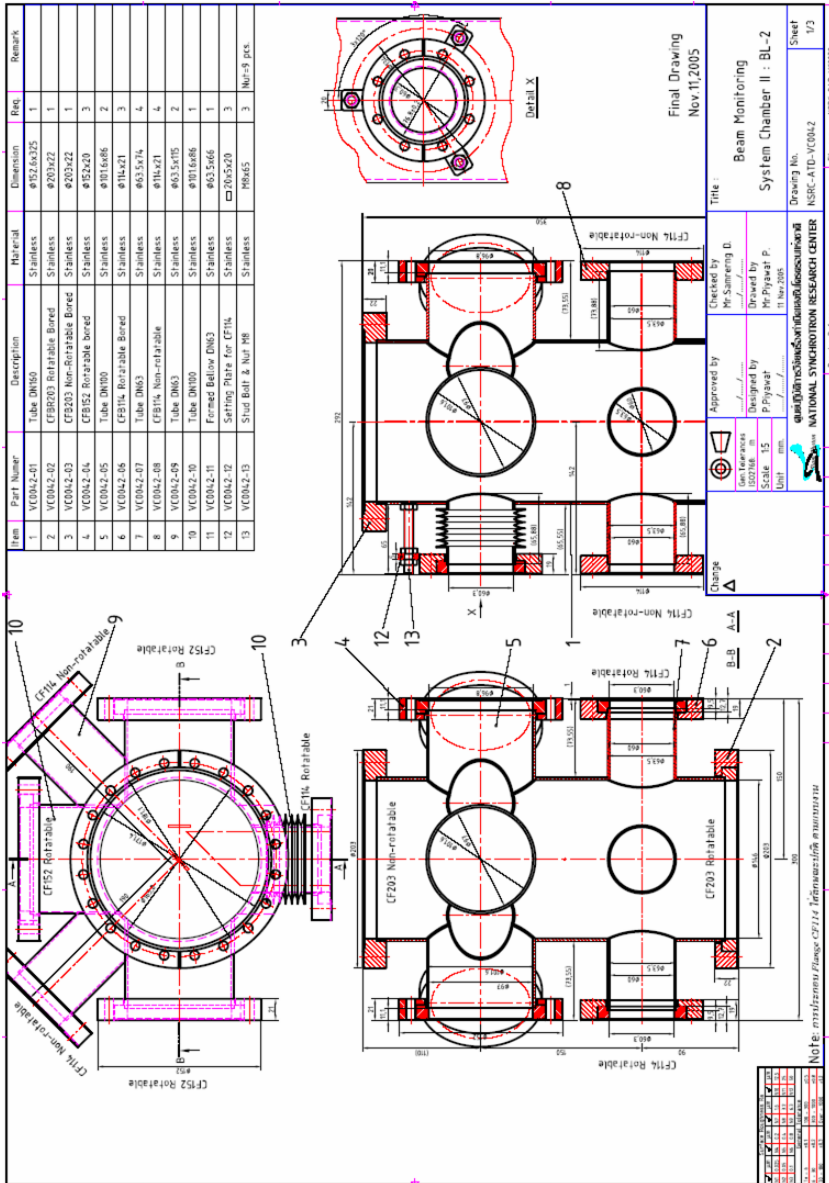
A2. Beam parameters list (Continued)

Name	betax(m)	alphax	dnux	etax(m)	etap(mr)	betay(m)	alphay	dnuey	s(m)
es19	6.138	2.892	4.269	0.921	-0.595	2.252	-1.172	2.623	73.77
d7	3.8	2.19	4.285	0.647	-0.595	3.554	-1.658	2.649	74.23
bm08	2.803	1.908	4.296	0.511	-0.526	4.42	-1.913	2.658	74.47
bm08	1.958	1.567	4.313	0.392	-0.453	5.41	-2.169	2.666	74.72
bm08	1.291	1.178	4.337	0.292	-0.376	6.525	-2.425	2.673	74.96
bm08	0.821	0.754	4.375	0.21	-0.297	7.764	-2.681	2.678	75.2
bm08	0.563	0.307	4.433	0.148	-0.215	9.127	-2.937	2.683	75.44
bm08	0.524	-0.15	4.507	0.106	-0.132	10.614	-3.193	2.687	75.69
bm08	0.707	-0.6	4.572	0.084	-0.048	12.225	-3.449	2.69	75.93
bm08	1.105	-1.04	4.616	0.083	0.037	13.96	-3.704	2.693	76.17
bm08	1.707	-1.44	4.644	0.102	0.122	15.82	-3.96	2.696	76.41
d6	3.095	-2.14	4.671	0.149	0.122	19.056	-4.37	2.699	76.8
qd28	5.87	-7.22	4.684	0.211	0.27	16.746	10.859	2.702	77.13
d5	8.942	-8.95	4.688	0.262	0.27	12.876	9.509	2.704	77.32
sv12	8.942	-8.95	4.688	0.262	0.27	12.876	9.509	2.704	77.32
d4	12.392	-10.5	4.691	0.31	0.27	9.732	8.253	2.707	77.49
qf18	16.043	0.228	4.694	0.355	0	6.969	1.024	2.713	77.82
d3	15.967	0.217	4.696	0.355	0	6.626	0.973	2.717	77.99
es20	15.967	0.217	4.696	0.355	0	6.626	0.973	2.717	77.99
d2	15.896	0.206	4.698	0.355	0	6.308	0.924	2.721	78.16
sh16	15.896	0.206	4.698	0.355	0	6.308	0.924	2.721	78.16
d1	15.247	0	4.73	0.355	0	3.403	0	2.84	81.3

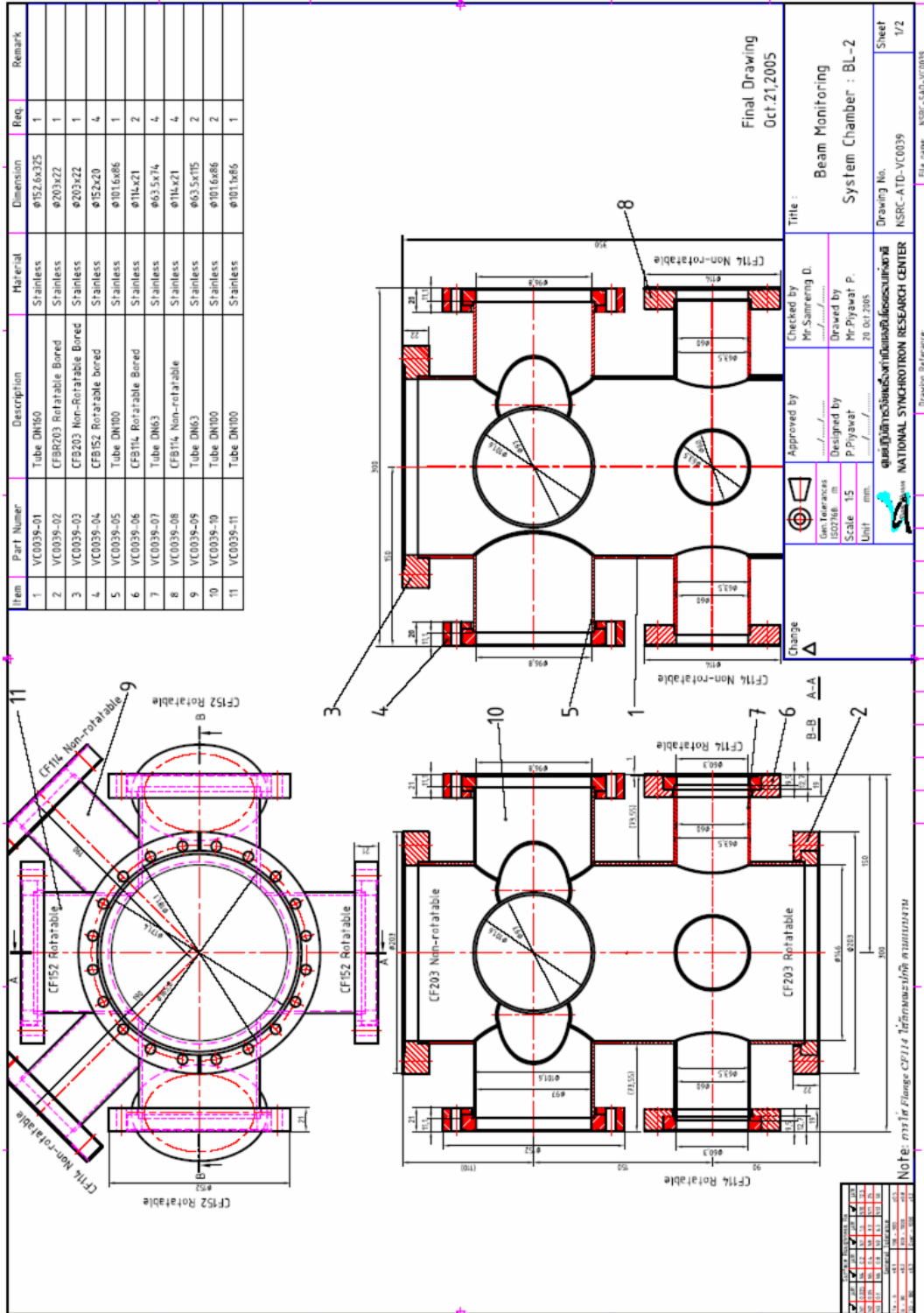
APPENDIX B

DRAWING

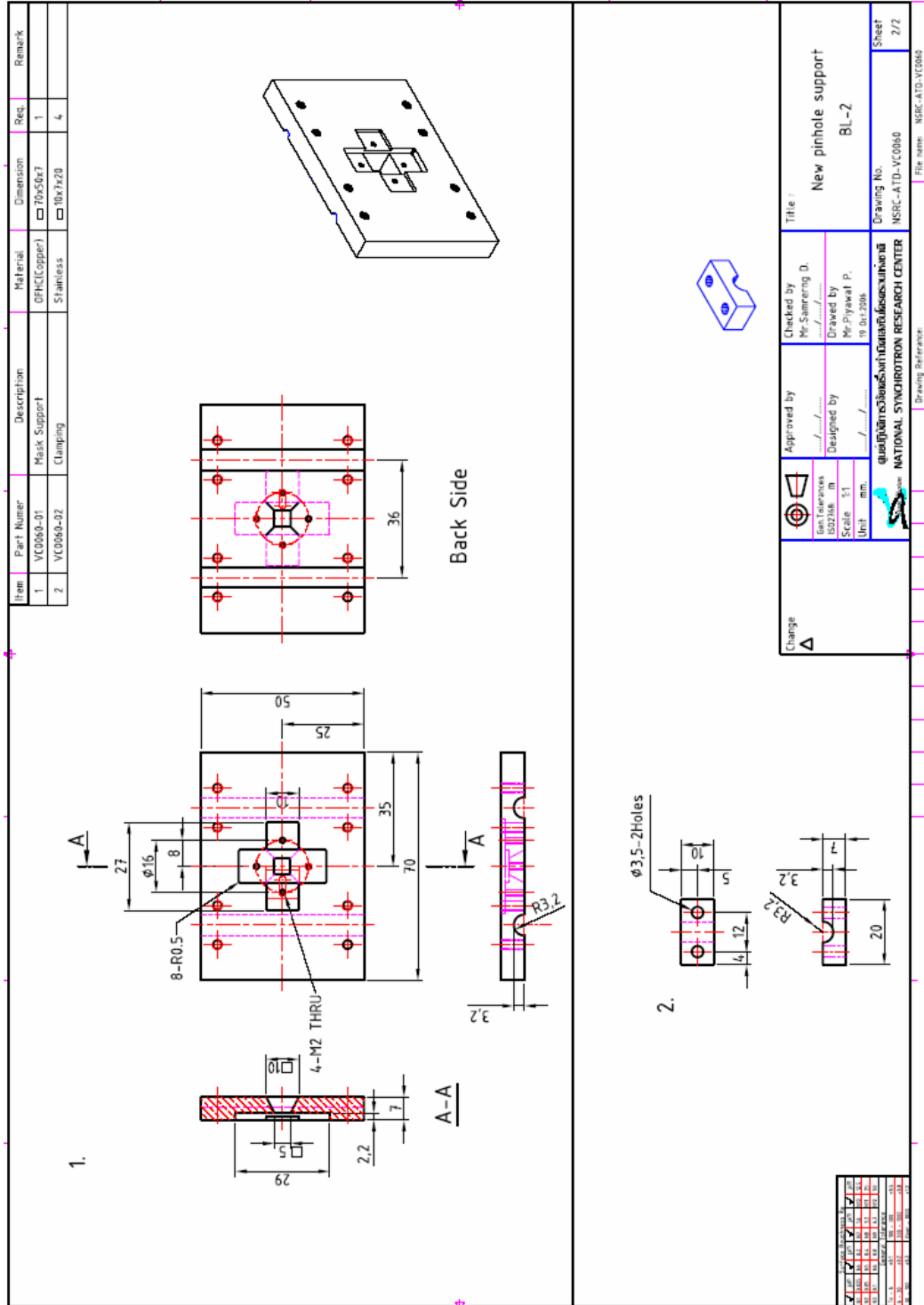
B1. The vacuum chamber 1



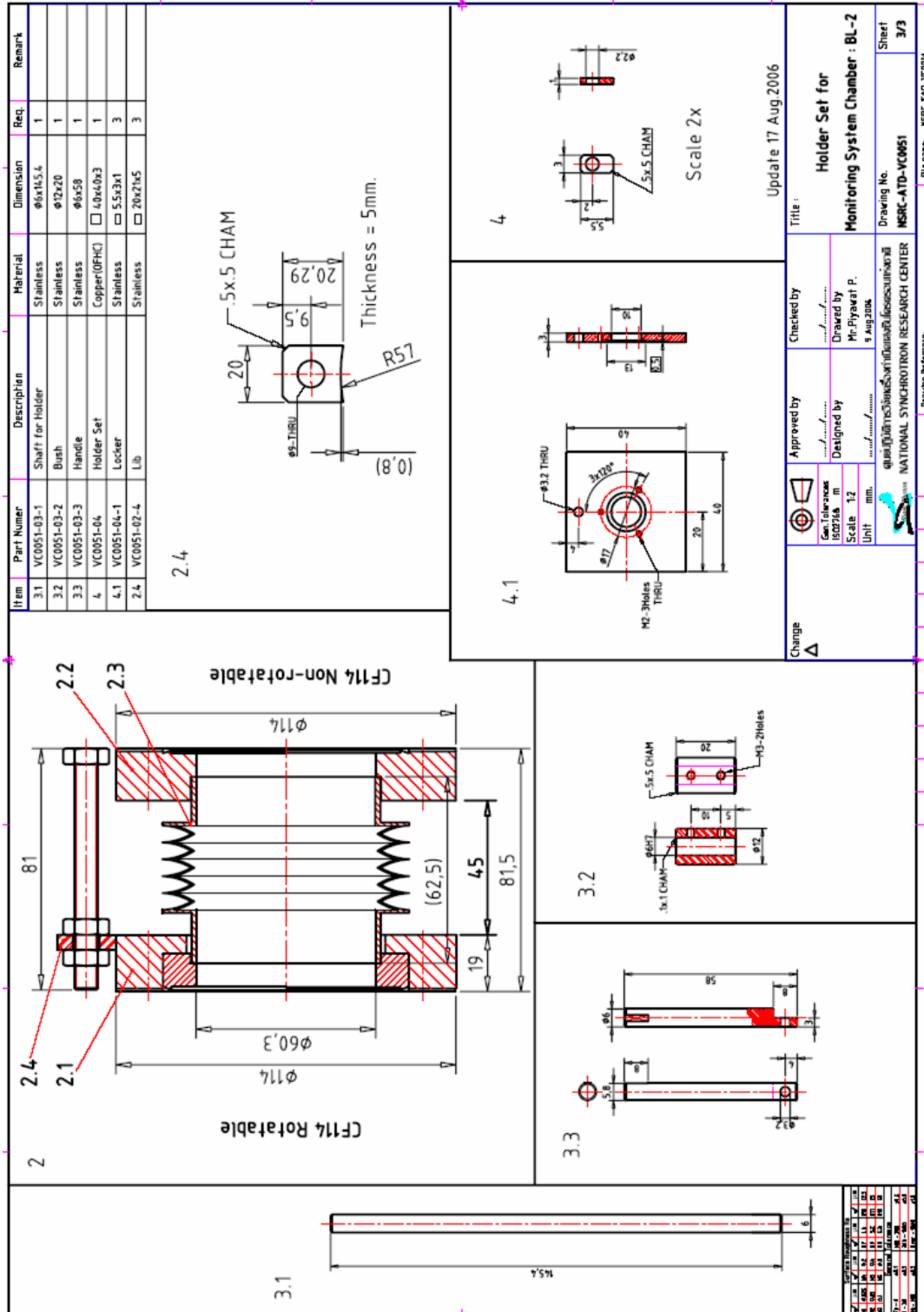
B2. The vacuum chamber 2



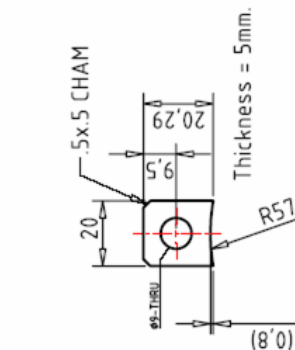
B3. X-ray pinhole



B4. YAG screen support 1



Item	Part Number	Description	Material	Dimension	Req.	Remark
3.1	VC0051-03-1	Shaft for Holder	Stainless	$\phi 6 \times 145,4$	1	
3.2	VC0051-03-2	Bush	Stainless	$\phi 12 \times 20$	1	
3.3	VC0051-03-3	Handle	Stainless	$\phi 6 \times 58$	1	
4	VC0051-04	Holder Set	Copper(DPHC)	$4 \times \phi 4 \times \phi 3$	1	
4.1	VC0051-04-1	Locker	Stainless	$5,5 \times 3 \times 1$	3	
2.4	VC0051-02-4	Lib	Stainless	$20 \times 2 \times 5$	3	



Change Δ

Approved by: _____
Checked by: _____
Designed by: Mr. Piyaat P.
Drawn by: _____
Unit: mm.
Scale: 1:2
Gen. Tolerance: ISO 2768 m
Date: 8 Aug 2006

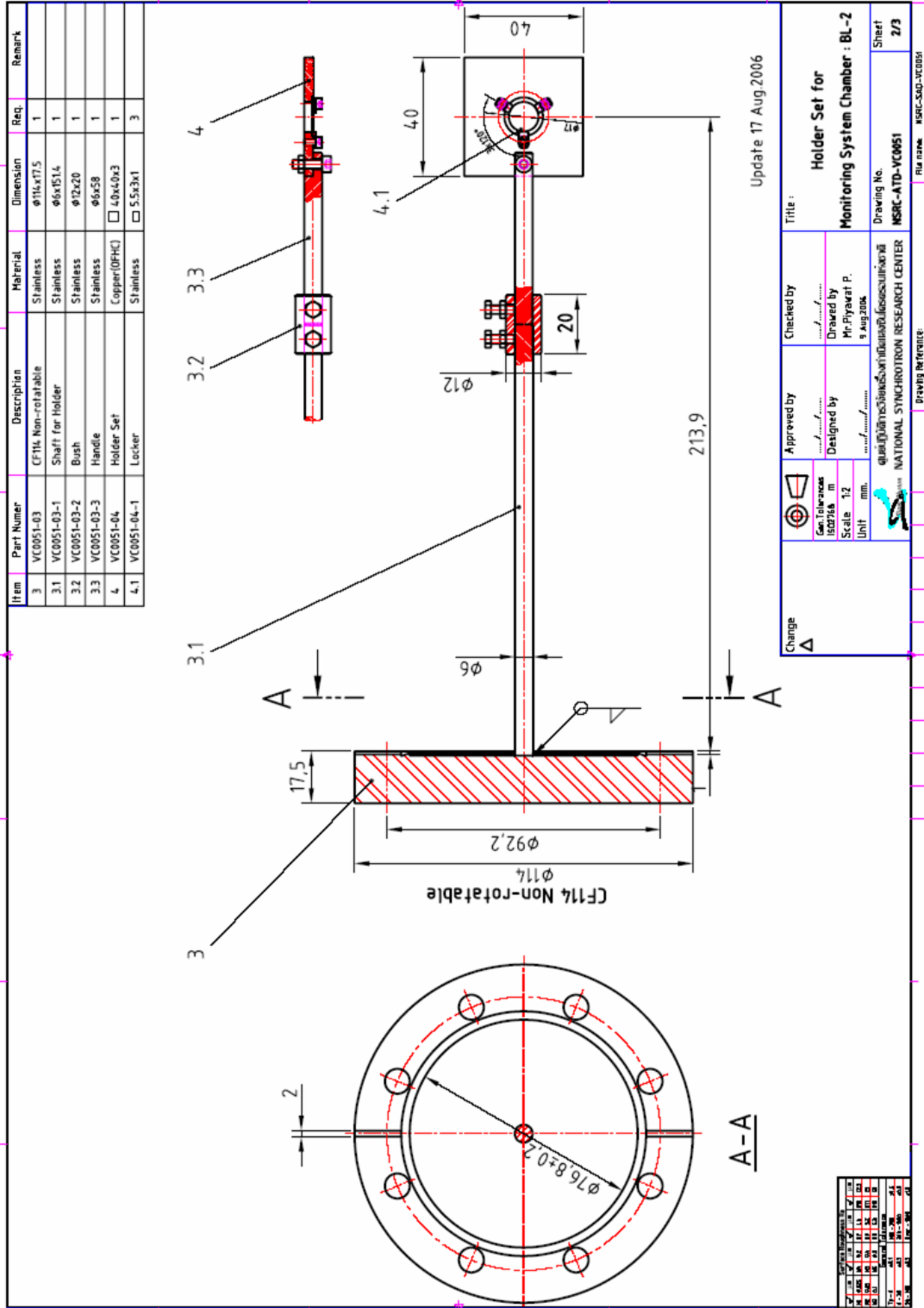
Title: Holder Set for Monitoring System Chamber : BL-2

Update: 17 Aug 2006

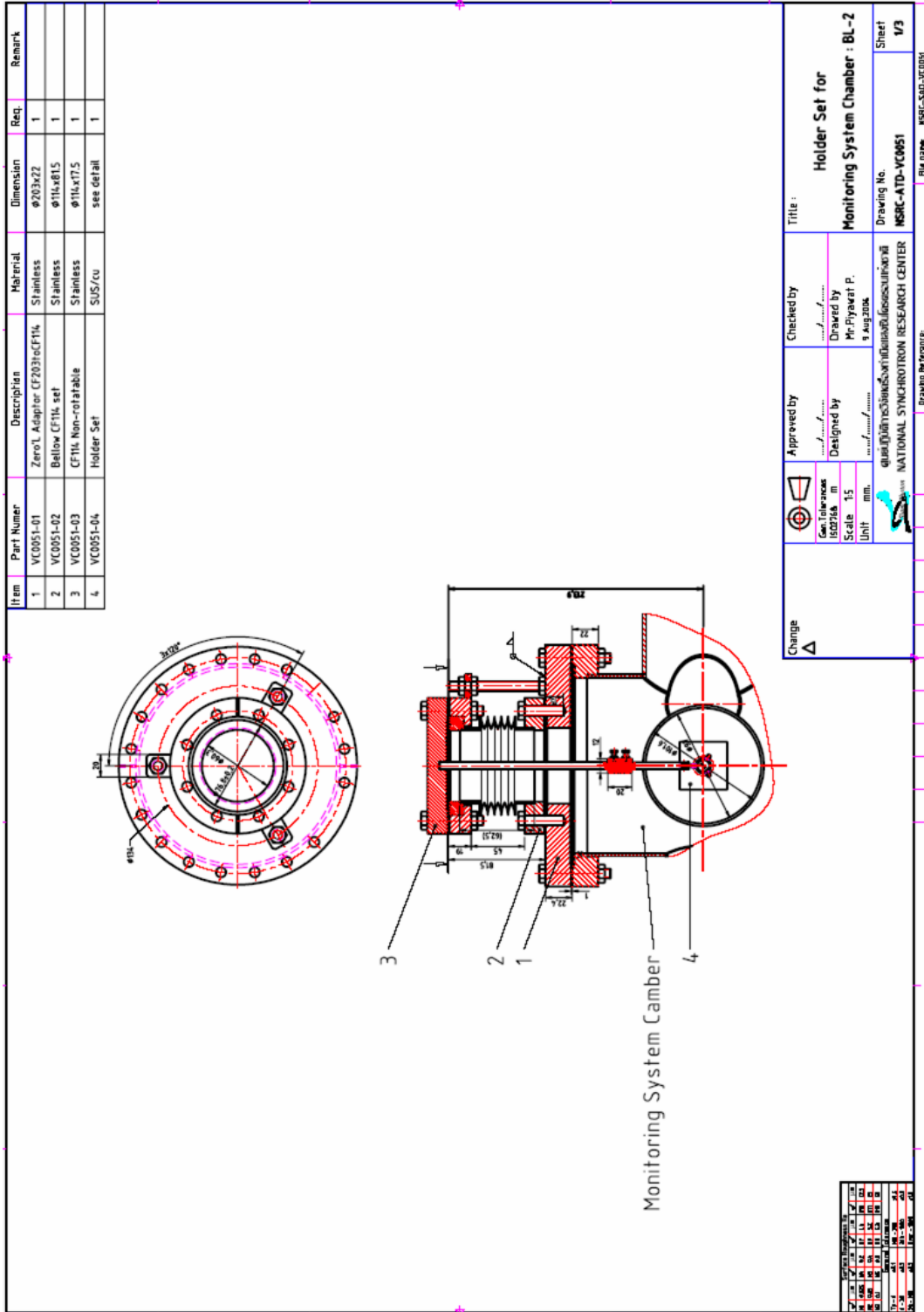
Drawing No. NSRC-ATD-VC0051
Sheet 3/3
Rev name: NSRC-SAO-VC0051

Rev.	By	Check	Date	Description
1	SAO	SAO	17/08/06	Issue for manufacturing
2	SAO	SAO	17/08/06	Update drawing
3	SAO	SAO	17/08/06	Update drawing
4	SAO	SAO	17/08/06	Update drawing
5	SAO	SAO	17/08/06	Update drawing
6	SAO	SAO	17/08/06	Update drawing
7	SAO	SAO	17/08/06	Update drawing
8	SAO	SAO	17/08/06	Update drawing
9	SAO	SAO	17/08/06	Update drawing
10	SAO	SAO	17/08/06	Update drawing
11	SAO	SAO	17/08/06	Update drawing
12	SAO	SAO	17/08/06	Update drawing
13	SAO	SAO	17/08/06	Update drawing
14	SAO	SAO	17/08/06	Update drawing
15	SAO	SAO	17/08/06	Update drawing
16	SAO	SAO	17/08/06	Update drawing
17	SAO	SAO	17/08/06	Update drawing
18	SAO	SAO	17/08/06	Update drawing
19	SAO	SAO	17/08/06	Update drawing
20	SAO	SAO	17/08/06	Update drawing

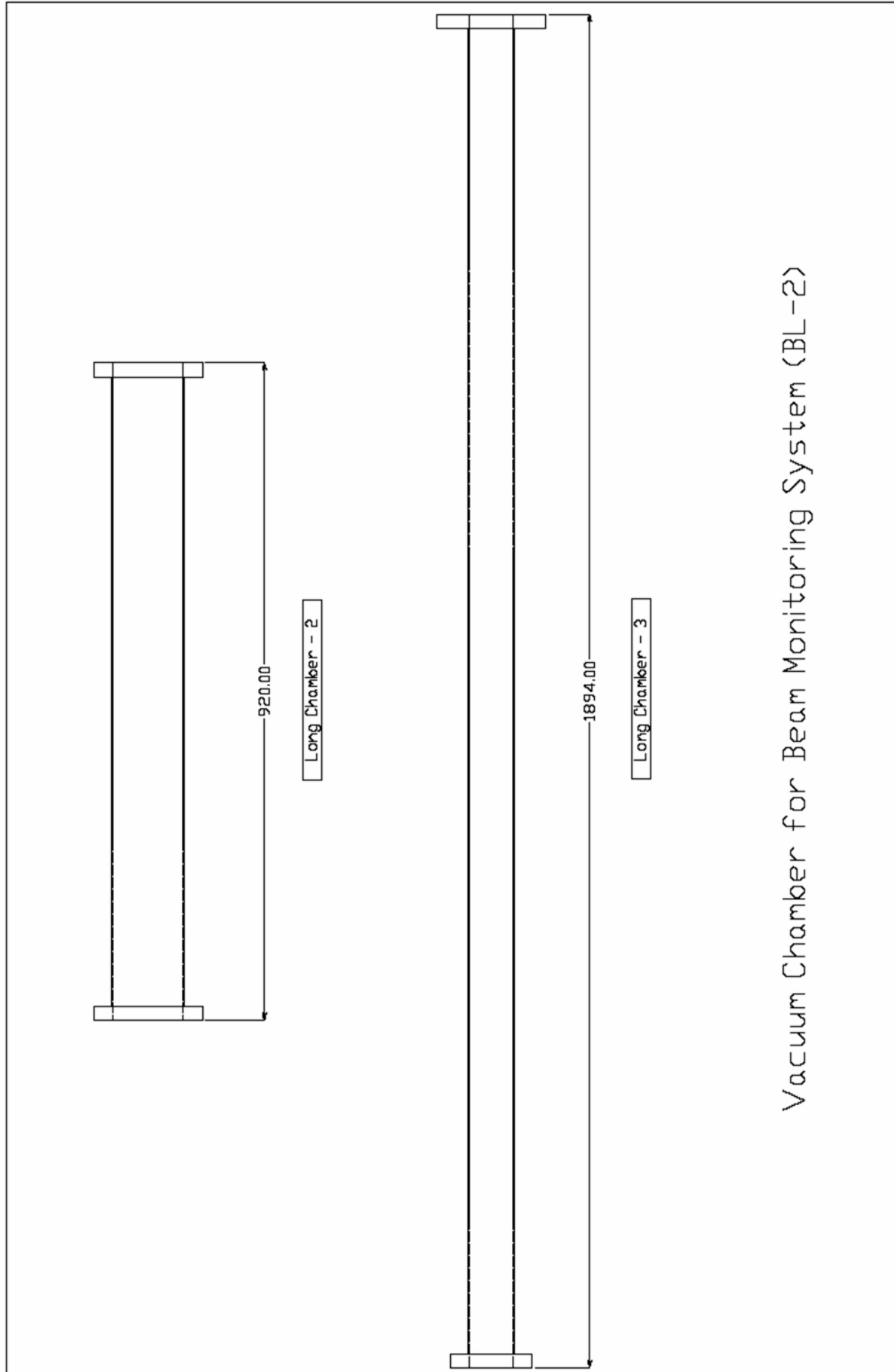
B5. YAG screen support 2



B6. YAG screen support 3



B6. Long vacuum chamber tube



APPENDIX C

THE MATLAB BEAM ANALYSIS PROGRAM

```
% Beam profile analysis (Version 0.2)

% This file is a "*.m" mat lab routine for analyze the
% electron beam profile taken by the beam monitoring system
% at the Siam Photon Source.

% Begin the routine
clear all;
more off;

ybgcutoff = 50; % define the region for y-background calculation
xbgcutoff = 50; % define the region for x-background calculation
x_micron_per_pixel = double(41.67); % Calibration parameter form CCD
y_micron_per_pixel = double(41.67); % Calibration parameter form CCD
magnification = double(1.74); % XPI magnification factor

% Initiallize beam parameters
cf_x = x_micron_per_pixel/magnification; % x-Size conversion factor
cf_y = x_micron_per_pixel/magnification; % y-Size conversion factor
fwhm_x = double(0.0);
fwhm_y = double(0.0);
beamsize_x = double(0.0);
beamsize_y = double(0.0);
sbeamsize_x = double(0.0);
sbeamsize_y = double(0.0);

dummy = double(0.0); % Dummy variable

% Step 1 : Load the image file

I = imread('profile1-grey.bmp');

% Convert the data to double type
% Initialize 2 D matrix named "Z". This is the image matix.

Z = double(I) + 1;
```

```

% Find the image dimensions
[ymax, xmax] = size(Z);
xm = int16(xmax);
ym = int16(ymax);

X = zeros(1,xm);    % Horizontal beam profile
Y = zeros(1,ym);    % Vertical beam profile

Xf = zeros(1, xm, 'double');  % x-Array for Gaussian Fitting
Yf = zeros(1, ym, 'double');  % y-Array for Gaussian Fitting

% Step 2 : Plot the beam image (top left)
subplot(2,2,1)
axis image;
    %colormap( 'gray' )
image(Z/4);

    %colorbar('EastOutside')
    %colorbar('YTickLabel',...
    % {'Freezing','Cold','Cool','Neutral','Warm','Hot','Burning'})
drawnow;

% Step 3 : Generate the vertical beam profile (top right)
subplot(2,2,2)

% Trow away the last column due to high accumulation of charges on CCD
xend = xm-1;

for j = 1:ym
    for i = 1:xend
        Y(1,j) = Y(1,j)+Z(j,i);
    end;
end;
sumbgy = 0;
for j = 1:ybgcutoff
    sumbgy = sumbgy + Y(1,j);
end;

bgy = sumbgy/ybgcutoff; % calculate average y-background
for j = 1:ym
    Y(1,j)= Y(1,j)- bgy; % subtracting y-background
    if Y(1,j) < 0
        Y(1,j) = 0;
    end;
end;
[dmy,jy] = max(Y); % find the vertical position of the beam center

```

```

% Calculation of FWHM(y)
half_dmy = dmy/2;
for j = 1:jy
    if (Y(1,j) < half_dmy)
        left_yj = j;
    end;
end;
for j = jy:ym
    if (Y(1,j) > half_dmy)
        right_yj = j;
    end;
end;
fwhm_y = right_yj - left_yj;

% Calculation of vertical beamsize

beamsize_y = double(fwhm_y)/2.35; % y-beam size in pixel
by2 = 2.0*(beamsize_y)^2;
sbeamsize_y = beamsize_y*cf_y; % y-beam size in micron

% Calculate the fitting Gaussian curve

for j = 1:ym
    dummy = double(j)-jy;
    dummy = (dummy)^2;
    Yf(1,j) = -dummy/by2;
end;
Yf = dmy*exp(Yf);

hold on
plot(Y, '-b',...
     'LineWidth', 2)
plot(Yf, '-r',...
     'LineWidth', 2)
h = legend('y-Data', 'y-Fitted', 2);
set(h, 'Interpreter', 'none')
axis tight
grid on
view(90, 90)
set(gca, 'XTick', 0:100:ym)
xlabel(['\fontname{times} Vertical FWHM = ',...
       num2str(fwhm_y), ' pixel'],...
       'FontSize', 12)
ylabel('Integrated intensity')
title(['\fontname{times} Vertical Beamsize = ',...
       num2str(sbeamsize_y, '%10.0f'), ' \mum'],...
       'FontSize', 14)

```

```
hold off;
drawnow;
```

```
% Step 4 : Generate the horizontal beam profile (bottom left)
subplot(2,2,3)
```

```
for i = 1:xend
    for j = 1:ym
        X(1,i) = X(1,i)+Z(j,i);
    end;
end;
X(1,xm) = X(1,xend); % copy the last colum data
```

```
sumbgx = 0;
for i = 1:xbgcutoff
    sumbgx = sumbgx + X(1,i);
end;
```

```
bgx = sumbgx/xbgcutoff; % calculate average x-background
```

```
for i = 1:xm
    X(1,i) = X(1,i) - bgx; % subtracting x-background
    if X(1,i) < 0
        X(1,i) = 0;
    end;
end;
```

```
[dmx,ix] = max(X); % find the horizontal position of the beam center
```

```
% Calculation of FWHM(x)
```

```
half_dmx = dmx/2;
for i = 1:ix
    if (X(1,i) < half_dmx)
        left_xi = i;
    end;
end;
for i = ix:xend
    if (X(1,i) > half_dmx)
        right_xi = i;
    end;
end;
fwhm_x = right_xi - left_xi;
```

```
% Calculation of beamsize
```

```
beamsize_x = double(fwhm_x)/2.35; % x-beam size in pixel
bx2 = 2.0*(beamsize_x)^2;
sbeamsize_x = beamsize_x*cf_x; % x-beam size in micron
```



```

% Calculate the fitting Gaussian curve

for i = 1:xm
    dummy = double(i)-ix;
    dummy = (dummy)^2;
    Xf(1,i) = -dummy/bx2;
end;
Xf = dmx*exp(Xf);

hold on
plot(X, '-b',...
     'LineWidth', 2)
plot(Xf, '-r',...
     'LineWidth',2)
h = legend('x-Data','x-Fitted',2);
set(h,'Interpreter','none')
axis tight
grid on
view(0, 90)
set(gca,'XTick',0:100:xm)
xlabel(['\fontname{times}Horizontal FWHM = ',...
       num2str(fwhm_x),' pixel'],...
       'FontSize', 12)
ylabel('Integrated intensity')
title(['\fontname{times}Horizontal Beamsize = ',...
       num2str(sbeamsize_x,'% 10.0f'),' \mum'],...
       'FontSize',14)
hold off;
drawnow;

% Step 5 : Generate the vertical beam profile (top right)
subplot(2,2,4)

axis auto;
% For gray scale use --> colormap( 'gray' );
colorbar('EastOutside');
colorbar('YTickLabel',...
        {'Very Faint','Faint','Dim','Neutral','Bright','Very Bright'})
surface(Z,'EdgeColor', 'y', 'FaceColor','default');
hold on;
shading interp;

%Rendering routine

lightangle(-45,10)
set(gcf,'Renderer','zbuffer')

```

```
set(findobj(gca,'type','surface'),...
'FaceLighting','phong',...
'AmbientStrength',.3,'DiffuseStrength',.8,...
'SpecularStrength',.9,'SpecularExponent',25,...
'BackFaceLighting','unlit')

% Yellow contour on the 3D profile --> contour3(X,Y,Z,25,'-y');

view(-30,30);
axis([0 (xmax-1) 0 (ymax-1) -150 255]);

% Draw countour on the bottom of 3D profile

meshc(Z);
hold off;

% End of the routine
```

CURRICULUM VITAE

Mr. Noppadon Deethae

Date of birth: 27 November 1978

Place of birth: Suphanburi, Thailand.

Nationality: Thai

Education

Academic year

1997-2000 Naresuan University, Phitsanulok, Thailand

Bachelor of Science (Physics)

2004-2007 Currently enrolling in Master majoring in School of Physics

Institute of Science, Suranaree University of Technology,

Nakhon Ratchasima, Thailand